# Retromer retrieves the Wilson Disease protein ATP7B from endolysosomes in a copper-dependent mode

Santanu Das[1], Saptarshi Maji*[1], Ruturaj*[1], Indira Bhattacharya[1], Tanusree Saha[1], Nabanita Naskar[2], Arnab Gupta[1,#]

[1]Department of Biological Sciences, Indian Institute of Science Education and Research Kolkata, Mohanpur-741246, India

[2]Chemical Sciences Division, Saha Institute of Nuclear Physics, 1/AF Bidhannagar, Kolkata-700064, India

* Contributed equally

[#] Correspondence to Arnab Gupta: arnab.gupta@iiserkol.ac.in

Wilson disease protein, ATP7B maintains copper homeostasis in the liver. ATP7B traffics from trans-Golgi network to endolysosomes to export excess copper. Regulation of ATP7B trafficking to and fro endolysosomes is not well understood. We investigated the fate of ATP7B, post-copper export. At high copper ATP7B traffics primarily to acidic, active hydrolase (Cathepsin-B) positive endolysosomes and upon subsequent copper chelation, returns to trans-Golgi network. At high copper, ATP7B co-localizes with endolysosomal markers and with core member of retromer complex, VPS35. Knocking down VPS35 did not abrogate copper export function of ATP7B or its copper-responsive anterograde trafficking to vesicles; rather upon subsequent copper chelation, ATP7B failed to relocalize to TGN that was rescued by overexpressing wtVPS35. Overexpressing mutants of retromer complex associated proteins, Rab7 and COMMD1 yielded similar non-recycling phenotype of ATP7B. At high copper, VPS35 and ATP7B are juxtaposed on the same endolysosome and form a large complex that is stabilized by in-vivo photoamino acid labeling and UV-crosslinking. We demonstrate that retromer regulates endolysosome to TGN trafficking of copper transporter ATP7B and it is dependent upon intracellular copper.

Keywords: *ATP7B, retromer, VPS35, copper metabolism, endolysosome, Wilson disease*



**JCS Advance Online Article. Posted on 2 December 2020**

## Introduction

Lysosomes have traditionally been believed as a disposal organelle of the cell. A growing body of recent studies have implicated lysosomes as centers of cellular nutrient sensing and recycling (Abu-Remaileh et al., 2017);(Korolchuk & Rubinsztein, 2011);(Rabanal-Ruiz & Korolchuk, 2018). With advancement in lysosomal research, the border between endosome and lysosomes has become increasingly blurred. Fusion between late endosomes and lysosomes gives rise to acid hydrolase-active endolysosomes that is distinct from terminal inactive storage lysosomes (Bright et al., 2016). There are growing evidences that lysosomes regulate cellular homeostasis of various metals like, Cu, Zn and Fe ( Strochlic et al., 2007; Kurz et al., 2011; Kambe, 2011; Polishchuk et al., 2014; Blaby-Haas & Merchant, 2014). Copper, a transition metal serves as an essential micronutrient for biological system. It participates in redox reactions in different cellular metabolic pathways shuttling between Cu(II) and Cu(I) states (Uauy et al., 1998), where $Cu^{1+}$ is favored for normal physiological activities (Fahrni, 2013). Several proteins tightly regulate copper homeostasis and supplies bioavailable copper to the secretory pathway. Excess copper induces oxidative stress through Fenton reaction and hence is detrimental for living system (Gupta and Lutsenko, 2009). Copper homeostasis is primarily maintained by two Trans Golgi Network (TGN) recycling P-type ATPase ATP7A (Menkes Disease Protein) and ATP7B (Wilson Disease Protein). ATP7A is expressed ubiquitously whereas expression of ATP7B is limited to liver, brain and kidney (Telianidis et al., 2013). ATP7B solely functions to maintain the copper homeostasis in hepatocytes (Muchenditsi et al., 2017). Defects in ATP7B leads to Wilson Disease (WD), a disorder characterized with copper accumulation in liver, brain and other organs manifesting severe hepatic or neurological symptoms (Huster and Lutsenko, 2007).

In this study we have attempted to dissect the copper-responsive trafficking itinerary of ATP7B and its mode of regulation in hepatocytes. At physiological/ basal copper level, ATP7B primarily resides on membrane of Trans Golgi Network (TGN) and functions in secretory pathway by delivering copper to Cu-dependent ferroxidase, ceruloplasmin (Lutsenko, 2016). At higher intracellular copper it vesicularizes (anterograde trafficking), sequestering copper inside vesicles and exports copper in lysosomes (Polishchuk et al., 2014). What is the fate of copper in the lysosome is still to be determined. It is possible that the entire copper in the lysosome is excreted out of the cell by exocytosis.

Alternatively, lysosomes may act as storehouse of bioavailable copper that is tapped as per the requirement of the cell.

Some recent and early studies have shown that membrane cargoes recycle back from lysosomes and endolysosomes (Seaman, 2007; Canuel et al., 2008; Suzuki and Emr, 2018a). We examined the fate of ATP7B at the lysosome/endolysosomes. We specifically asked (a) does ATP7B shows a preferential localization at acid-hydrolase-active endolysosomes or at inactive storage endolysosomes or (a) Is ATP7B degraded at those compartments during its copper export activity and (b) If not, what is the mechanism that retrieves ATP7B from endolysosomal/lysosomal compartments?

Over 300 mutations in ATP7B are associated with WD and are frequently used to understand regulation and structure-function correlation of ATP7B ( Forbes and Cox, 1998; Caca et al., 2001; Cox et al., 2005; Gupta et al., 2005; Abdelghaffar et al., 2008; Aggarwal et al., 2013; Braiterman et al., 2014; Ala et al., 2015). These disease mutations affect the functioning of ATP7B either by affecting its copper transporting activity or its trafficking or both ( Gupta et al., 2011; Braiterman et al., 2014). Several proteins govern trafficking and stability of ATP7B (Materia et al., 2012; Jain et al., 2015); reviewed in (Gupta et al., 2018) that interact directly or indirectly with defined and conserved motifs of the protein. These motifs influence the directionality of cargo transport between organelles like Golgi-endosome-plasma membrane.

Although the anterograde pathway of ATP7B has been moderately well characterized (Braiterman et al., 2009; Gupta et al., 2016; Polishchuk et al., 2014), the regulation which mediates its retrograde transport from lysosomes/endolysosomes has been elusive. Recent studies have shown that retromer regulates retrieval or rescue of cargoes from endosomal and lysosomal compartments (Burd and Cullen, 2014**;** Gershlick and Lucas, 2017; Tammineni et al., 2017).Retromer is a highly conserved endosomal sorting complex, composed of core components, Vacuolar Protein Sorting, VPS35, 26 and 29 and variable components, Sorting Nexins (SNX) along with WASH complex, that are involved in retrograde transport of endocytosed transmembrane proteins (cargoes) to the trans-Golgi network (TGN) or cell surface (Seaman, 2018; Suzuki et al., 2019). Studies from Burd group have provided a mechanistic understanding of retromer oligomerization and cargo sorting (Deatherage et al., 2020; Ma et al., 2020) (summarized in the review (Burd and Cullen, 2014). Harrison et al shown that membrane recruitment of retromer is mediated by bivalent recognition of an effector of PI3K, SNX3, and the GTPase, Rab7 by the VPS35 retromer subunit. These interactions facilitates retromer to bind integral membrane cargo

leading to membrane binding of retromer and subsequent cargo sorting (Harrison et al., 2014). Studies by Seaman has determined the role of retromers on recycling of the CI-M6PR, the protein which delivers acid hydrolases to lysosome from TGN (Seaman, 2004**;** Seaman, 2007). Studies from Emr and co-workers have shown that in yeast proteins like autophagy protein Atg27 is recycled from vacuole to the endosome via the Snx4 complex and then from the endosome to the Golgi via the retromer complex (Suzuki and Emr, 2018b). Further they have also demonstrated that both VPS26 and VPS35 are critical in cargo retrieval; however VPS26 utilizes different binding sites depending on the cargo, allowing flexibility in its cargo selection (Suzuki et al., 2019). Besides TGN delivery, retromers also regulate endosome-to-plasma membrane recycling as in copper transport, CTR1 (Curnock and Cullen, 2020).

In this study, we have demonstrated that at elevated intracellular copper, the Cu-P-type ATPase, ATP7B, localizes primarily on the active acid hydrolase (Cathepsin B)-positive endolysosomes. Subsequently, upon copper chelation, it recycle to TGN and this phenomenon is regulated by the retromer. We have demonstrated that similar to as in case of an 'endocytic cargo' (Mellado et al., 2014; Tabuchi et al., 2010)retromer also sorts the 'secretory cargo', i.e., ATP7B for its TGN delivery from endolysosomes and late endosomes.

## Results

### ATP7B recycles between endolysosomes and trans-Golgi Network in a copper dependent manner

- ATP7B vesicularizes from trans-Golgi network in response to high copper and recycles back to TGN upon copper chelation (Roelofsen et al., 2000). To determine the optimal time of recycling of ATP7B from vesicles to TGN, HepG2 cells (human hepatocellular carcinoma cell line) were treated with high copper (50µM; 2h) and subsequently treated with 50µM BCS (Bathocuproine disulfonic acid), a copper chelator for varying time periods (10min, 30min and 2h). Gradual increase in colocalization between TGN and ATP7B was observed with 10mins, 30mins and 2h of BCS treatment post high copper as evident from Pearson's Colocalization Coefficient (PCC). At 2h, maximum TGN retrieval of ATP7B was observed (Fig. 1, A and B).

Polishchuk et al have demonstrated that ATP7B utilizes lysosomal exocytosis to export copper (Polishchuk et al., 2014). We investigated whether ATP7B degrades at the lysosome after it transports copper or it recycles back from these compartments for a next

round of export cycle. We treated the cells with either BCS (50µM) or copper (50µM). Using immunofluorescence assay we determined that under high copper conditions ATP7B exits TGN and colocalizes with endolysosomal markers Lamp1 (Fig. 2A,B) and Lamp2 (Fig. S1A,B) and to a lesser extent with late endosome, i.e., Rab7 positive compartments (Fig.S2A,B). Upon copper chelation using BCS, ATP7B recycled back to TGN from endolysosomes and late endosomes (bottom panel images of Fig. 2A, and Fig. S1A, & S2A). We did not observe its appreciable colocalization with the recycling endosomal marker Rab11 (Fig S2C,D).

Lamp1 typically marks the terminal end of the endolysosomal pathway (Humphries et al., 2011), but frequently, Rab7 and Lamp1 also co-labels the non-degradative lysosomal compartment (Cheng et al., 2018). To determine the percentage distribution of ATP7B in the milieu of late endosomal-endolysosome compartments (Rab7-Lamp1), we utilized Structured Illumination Microscopy (SIM) along with deconvolution confocal microscopy imaging. At elevated copper (50µM) we found a proportionately higher co-distribution of ATP7B with compartments positive for both Rab7 and Lamp1 than compartments positive for individual markers. At this condition, 48.5% ± 13.2 of total cellular pool of ATP7B colocalized with either Lamp1 or Rab7 or both. Among them, 44.9% ± 14 of ATP7B localized in vesicles positive for both Lamp1 and Rab7. Hence, it is inferred that recycling of ATP7B to TGN upon Cu chelation is largely from vesicles which are positive for both the markers (Fig. S3A and 3B). Together this result suggests that ATP7B localizes at endolysosomal compartments at high copper.

We wanted to scrutinize the nature of the ATP7B-harboring endolysosomal compartment with respect to its hydrolase activity. The delivery of macromolecules for degradation by lysosomal acid hydrolases requires traffic through early endosomes to late endosomes followed by fusions between late endosomes and lysosomes. Using Cathepsin-B substrate, Magic red (MR) that releases fluorescence reporters (Cresyl violet) upon proteolytic cleavage, Bright and co-workers have demonstrated that the late endosome-lysosome fusion results in the formation of acid-hydrolase-active endolysosomes, which are hybrid organelles and are distinct from inactive terminal storage lysosomes (Bright et al., 2016). We employed this technique to identify the ATP7B-residing compartments at high copper. Cells were treated with Dextran A- Alexa 647 and Magic Red. The total lysosomal pool was labeled with Dextran A-Alexa 647 (far red) and acid hydrolase active fraction was stained red due to the hydrolase-mediated release of the fluorescent reporter, Cresyl violet ($\lambda_{em}$ 622nm) (Fig. 2C and Fig. S4). We noticed that ATP7B at high copper

(50µM and 250µM) distributes between active lysosomes and storage lysosomes with a higher abundance in the active ones. Interestingly, compared to at 50µM copper, at 250µM, the percentage localization of ATP7B, though stayed constant at the active lysosomes, increased ~50% in the storage lysosomes (Fig.2D). This increase might be attributed to further shift of ATP7B localization from the TGN to the endolysosomes with increasing copper. However, there were no apparent degradation of ATP7B in either of the copper treatment conditions as evidences in immunoblots (Fig. 2E) No evidence of degradation was also recorded in controls: Lamp1 (lysosomal marker), Na,K-ATPase (membrane protein marker) (Fig.2E &2F). Upon treatment with copper chelator, BCS, in presence of cyclohexamide, ATP7B returned to its tight perinuclear location reminiscent of TGN (Fig. 2Ci,Cii, lower panel images). Furthermore, using live cell imaging in HepG2 cells, we confirmed the dynamic fusion and fission of GFP-wtATP7B vesicles with/from dual stained (DexA in blue and Magic Red in red) active hydrolase-positive endolysosome (marked with an arrowhead and that region is magnified in a box in video1). Image capture was initiated at the point of copper treatment and data was collected at an interval of 5s for a total period of 15 mins.

It is worth mentioning that the size and shapes of the Lamp1 positive vesicles are variable across cells and as well as in a single cell. It varies from 20-200µM in diameter (maximum length across) and shape varies from small puncta to larger patchy clumps. We noticed that abundance of Lamp1 positive compartments was higher in cells treated with copper than untreated cells.

**Retromer regulate retrograde trafficking of ATP7B from endolysosomes**

It has been shown that Menkes disease protein, ATP7A, the homologue of ATP7B require SNX27-retromer to prevent lysosomal degradation and maintain surface levels and localization (Steinberg et al., 2013). Also, CI-M6PR recycles between TGN and endosomes in a retromer regulated fashion to sort lysosomal hydrolases (Seaman, 2004; Seaman, 2007; Arighi et al., 2004; Cui et al., 2019). ATP7B exits endolysosomal compartments by an unknown regulatory mechanism upon copper chelation. This prompted us to investigate if the retromer complex plays a role in retrieval of ATP7B from endolysosome and late endosomal compartments. VPS35 is the largest core component of the retromer complex. It functions as the scaffold for the assembly of other core components, VPS29 and VPS26 and also cargo binding (Hierro et al., 2007). Hence, we selected hVPS35 as the target component to determine the role of retromer complex, if any in copper mediated trafficking of ATP7B. Broadly, localization and trafficking of ATP7B

in HepG2 can be divided in 4 *phases (a)* at the TGN in Basal Cu (or –Cu), *(b)* on the anterograde vesicles in high Cu (50µM for 2h) and *(c)* Subsequently upon copper chelation: on the retrograde vesicles (10 mins, 50µM BCS treatment) and *(d)* further, majority of ATP7B recycled back to the TGN in copper chelated conditions (30 mins, 50µM BCS treatment).

Immunoblot analysis of VPS26 and VPS35 revealed that HepG2 cells expresses the retromer complex proteins (Fig. 3A) and copper levels does not alter abundance of VPS35 in HepG2 cells (Fig. S5A). To study if ATP7B co-localizes with retromer core components, cells were treated with either of the 4 conditions described above. Cells were fixed, blocked and co-stained with anti-ATP7B and anti-VPS35 antibody. Maximum colocalization as quantified by Pearson's Colocalization Coefficient between VPS35 and ATP7B was observed in high copper (*phase b*) and in Cu (2h)>BCS (10min) (*phase c*) conditions. With 30 mins of BCS treatment post high copper (*phase d*), ATP7B and VPS35 shows loss of colocalization (Fig.3B &3C). Similar observations were made with VPS26 (data not shown).

To further understand if retromer regulates any of these phases of ATP7B trafficking, we knocked down VPS35 and studied the phenotype of copper induced localization of ATP7B with respect to TGN. Appreciable knockdown was attained (>70-80%) for the targeted siRNAs as compared to scrambled for VPS35 as ascertained by immunoblotting (Fig. 4A). Additionally, as reported by (Fuse et al., 2015) decrease in VPS26 level was also observed in VPS35 KD cell which eventually tells us expression as well as functionality of VPS subunits are interdependent (Fig.S5B). Recycling of CI-M6PR between Golgi and endolysosomes was used as a control to functionally evaluate knockdown of VPS35. As reported previously, we found that CI-M6PR localized in vesicles in cells transfected with siRNA against VPS35 KD as compared to scrambled RNA transfected cells where CI-M6PR shows a complete localization with TGN46 (Fig. S5C) (Seaman, 2007).

VPS35 siRNA treated cells were incubated with (a) BCS (2h) or (b) Copper (2h) or (c) Copper (2h)>BCS (30 min), fixed, blocked and stained with the anti-ATP7B and anti-Golgin97 antibodies. We observed that trafficking of ATP7B from the vesicles back to the TGN (*condition c*) was significantly abrogated (Fig.4B and 4C). ATP7B remained in vesicles and failed to recycle back to TGN even after the cells were incubated in BCS for a prolonged time of 2h subsequent to copper treatment (not shown).

To corroborate our finding that VPS35 regulates ATP7B trafficking, we utilized live cell imaging using the wild type and the inactive dominant negative mutant mCherry-VPS35 (R107A) (gift from Dr,Sunando Datta, IISER Bhopal). The R107A mutation abolishes the interaction of VPS35 with VPS26 and affects cargo sorting (Gokool et al., 2007);(Zhao et al., 2007). HEK293 cells were co-transfected with GFP-ATP7B and mCherry-wt-VPS35 and GFP-ATP7B was concentrated at TGN (perinuclear region) by preincubating the cells with copper chelator, BCS. Vesicularization and recycling of ATP7B was triggered with treatment with copper. Image capture was initiated at the point of copper treatment and data was collected at an interval of 1.964 second for a total period of 30 mins. We noticed that within 1 min of Cu treatment, GFP and m-Cherry signals colocalized at the same endosomal vesicle. The dwell time of wt-VPS35 and GFP-ATP7B on the vesicle was notably higher for wt-VPS35 compared to the mutant. For VPS35-R107A, the colocalization lasted for few seconds (4-11 seconds) but for wt-VPS35, the colocalization lasted for an average of 7 mins. (Video 2A and 2B) and (Fig. S6Ai,Aii).

Since we determined that ATP7B colocalizes at the endolysosomes at high copper, we investigated if VPS35 regulates endolysosomal exit of ATP7B on triggering its retrograde pathway. Using identical experimental conditions of knocking down VPS35 or not, we found that ATP7B colocalizes with VPS35 in high copper (Fig.S6B; left image, top and bottom panel) under both KD and control cells. ATP7B is arrested at Lamp1 positive compartments upon triggering the retrograde pathway (i.e., high copper > BCS) (Fig. S6B; center images, bottom panel) but not in Scrambled RNA treated cells (Fig. S6B, top panel). Boosting the retrograde pathway by lengthening BCS treatment time to 2h did not facilitate retrieval of ATP7B from the lysosomes (Fig. S6B right images, bottom panel), unlike control ((Fig. S6B right images, top panel).

We further confirmed the role of retromer by rescuing the non-recycling phenotype of ATP7B in VPS35 KD cells by overexpressing mcherry-wt-VPS35. We found that ATP7B recycled back from vesicular to its tight perinuclear TGN localization upon copper chelation in VPS35 KD cells that overexpressed the wt-VPS35 construct but not the mutant R107A-VPS35 or in untransfected cells (Fig. 4D). These experiments confirm that VPS35 regulates retrieval of ATP7B from endolysosomes to TGN upon copper depletion.

**Retromer-associated proteins Rab7 and COMMD1 regulates ATP7B recycling**

We explored the possible role of two proteins in retrograde trafficking of ATP7B that has been shown to interact directly or indirectly (as part of a complex) with the retromer. It has

been now been thoroughly established that Rab7 regulates recruitment of the core retromer trimer VPS35, 26 and 29 to the endosomal membrane and interference with Rab7 function causes dissociation of the trimer (Rojas et al., 2008). On other hand, COMMD1 protein, whose dysfunction phenocopies Wilson disease mutation, interacts with the WASH complex and is critical in copper dependent endosomal localization of the Cu ATPase ATP7A (Phillips-Krawczak et al., 2015) and retrograde trafficking of ATP7B (Miyayama et al., 2010). Interaction of the WASH complex with VPS35 is crucial for its endosomal localization and this facilitates cargo sorting by promoting formation of endosomal F-actin (Seaman and Freeman, 2014).

We overexpressed the dominant-negative mutant Rab7-T22N (impaired in nucleotide exchange and with a reduced affinity for GTP) (Spinosa et al., 2008) and studied its effect on retrograde trafficking of ATP7B. Trafficking of ATP7B was triggered with 50μM copper for 2h. Subsequently upon copper chelation, we observed that ATP7B stays vesicularized and fails to return to its perinuclear location in cells overexpressing the DN mutant, a phenotype that is identical to VPS35 KD condition (Fig.4Ei, bottom panel). Cells overexpressing Wt-Rab7 exhibited a normal trafficking itinerary of ATP7B (Fig.4Ei, upper panel)

We studied the effect of two COMMD1 mutants on retrograde trafficking of ATP7B. The COMMD1 mutation, T174M was discovered as a WD patient with deteriorating prognosis even after early medical intervention (Gupta et al., 2010). The other key residues mutated in COMMD1 were K167E/K173E, as the positively charged Lys was shown to be crucial for its phosphatidylinositol interaction (Burkhead et al., 2009), (Stewart et al., 2019). Cells were transfected with GFP-COMMD1-T174M or GFP-COMMD1 K167E/K173E and trafficking of ATP7B was triggered with 50μM copper for 2h. Subsequently upon copper chelation with BCS, we observed vesicular localization of ATP7B in cells over expressing either GFP-COMMD1-T174M or GFP-COMMD1 K167E/K173E (Fig.4Eii middle and bottom panel). Cells overexpressing Wt-COMMD1 exhibited a normal trafficking itinerary of ATP7B (Fig.4Eii top panel).

We conclude that interfering with the functioning of the retromer core proteins or proteins that are associated with the retromer complex abrogates the retrograde trafficking of ATP7B.

**Lysosomal luminal pH does not influence localization of ATP7B and recruitment of VPS35**

It emerges that copper induced localization of ATP7B involves a tripartite participation, i.e., ATP7B, endolysosome and retromer. After confirming the role of VPS35 in this process, we asked if luminal endolysosomal environment affect retromer recruitment and hence ATP7B retrieval from lysosome. Retromers have been previously implicated in lysosomal activity e.g., autophagy (Cui et al., 2019). We investigated if the targeting of ATP7B to lysosomes in high copper or its retrieval initiation by VPS35 recruitment is affected by inactivation of the V-ATPase that is crucial for lysosomal functioning. Cells were treated with the V-ATPase inhibitor, BafA1 (200nM), in 50µM copper for 2h (to trigger lysosomal targeting of ATP7B) and Cu>BCS (50µM, 20 mins) conditions to trigger its lysosomal exit and retrograde trafficking. No observable and significant difference in colocalization of Lamp1, ATP7B and VPS35 was obtained between BafA1 treated vs the control in either of the copper treatment condition (Fig. 5A,B). It can be inferred that retromer being situated on the outer membrane of the Lamp1 positive compartments is unaffected by the change in luminal pH of the lysosome brought on by BafA1 treatment. Localization of ATP7B also stays unaltered as also demonstrated by Polishchuk and co-workers. (Polishchuk et al., 2014).

**VPS35 acts on ATP7B in a micro-distant *modus operandi***

Next, using biochemical assays to investigate if VPS35 directly interacts with ATP7B we utilized co-immunoprecipitation where GFP-ATP7B was expressed in cells, pulled down with anti-GFP beads and probed for endogenous VPS35. At high copper (100 or 200µM) or upon subsequently triggering ATP7B recycling BCS (100 µM), we failed to detect any signal in the immunoblot at developed with anti-VPS35 antibody (Fig. S7 show data for Cu: 200µM and Cu (200µM) to BCS (100µM).

To understand the underlying reason of our inability to detect interaction between ATP7B and VPS35 using biochemical methods, we resorted to Super resolution microscopy to determine the exact positioning of ATP7B w.r.t VPS35 at the lysosomal compartment. Using Structured Illumination Microscopy and High resolution deconvolution confocal microscopy we observed that ATP7B and VPS35 lies in juxtaposition on the lysosomal compartment (stained with Lamp1 antibody) at high copper conditions (Fig.6A-D). The average distance between these two proteins varies from 25nm~200nm. It can be inferred that although ATP7B lies in close proximity to VPS35 and is regulated in its retrograde

pathway by retromer, the physical interaction between these two proteins are indirect. We utilized Stimulated Emission Depletion (STED) microscopy to look further closely on the disposition of ATP7B and Vps35 on a vesicular membrane. Using Z-stacking we determined the shape of a vesicle (dotted circle in Fig. 6E). At high copper, we observed that ATP7B (green) and Vps35 (red) decorated the vesicular membrane with a signal overlap (yellow) at a maximum resolution of 25nm further substantiating our biochemical findings.

Since, the interaction between ATP7B and VPS35 is likely to be indirect and possibly they a part of a larger complex, we utilized **P**roximity **L**igation **A**ssay (PLA) to substantiate our finding. Interaction of Hur and Trim21 (Guha et al., 2019) were used as positive controls and secondary antibodies against ATP7B (anti-rabbit) and VPS35 (anti-goat) were used as negative controls. We observed positive interaction between ATP7B and VPS35 that is evident by formation of red intracellular puncta on sites if the two proteins juxtapose at a distance less than ≤40nm (Fig. 6F).

This finding strongly suggest that VPS35 and ATP7B are a part of a larger complex and the regulation of ATP7B trafficking by the retromer proteins are possibly indirect and they do not share a physical interface. To detect such an interaction, we metabolically labeled GFP-ATP7B overexpressing HepG2 cells with Photo amino-acids (P-Leucine and P-Methionine). Cells were treated with copper (50µM for 2h) or copper chelator, BCS (50µM for 2h) and subjected to UV crosslinking. Crosslinked GFP-ATP7B complex was immunoprecipitated with anti-GFP beads. Upon probing the eluate on an immunoblot with anti-VPS35, anti-VPS26 and anti-GFP antibodies, a complex >> 250kDa was detected that was comprised of all the three proteins. The complex was found to be absent or much less abundant in cells treated copper chelator (Fig 6G).

**VPS35 knockdown does not abrogate copper export function of ATP7B**

We have now established that retromer regulates retrograde trafficking of ATP7B and that downregulation of VPS35 arrests ATP7B on endolysosomes. We examined if these ATP7B arrested on endolysosomes are capable of exporting copper. We knocked down VPS35 using lentiviral mediated shRNA delivery in HepG2 cells. Scrambled, non-targeting shRNA was used as control (Fig.S8A). shRNA# 2, 3 and 5 revealed significant knockdowns and hence were subsequently used for the experiment. Cells were either treated with 50µM copper for 2h or maintained at basal media. We did not observe any statistically significant change ($p>0.1$) in cell viability in either of the treatment conditions

as determined by Neutral Red (NR) assay (Fig. 7A). No apparent change in cell morphology was recorded in any of these conditions ascertained by 40X phase contrast microscopy (Fig. S8B). Copper measurement in these cells from four conditions (sh_Scrambled-Basal Cu, shVPS35-Basal Cu, sh_Scrambled-Cu50µM and shVPS35-Cu50µM) were carried out using inductively coupled plasma - optical emission spectrometry (ICP-OES). Interestingly, we found that upon copper treatment, accumulation of copper was significantly lower ($p<0.01$) in VPS35 KD cells as compared to non-KD control cells (Fig. 7B). This suggests that ATP7B arrested on the lysosomes in VPS35 KD condition is continuing its copper export function resulting in lower accumulation of intracellular copper. However, in basal condition, both VPS35 KD and control cells exhibited similar levels of intracellular copper (Fig.7B).

Recently, it has been shown that retromer regulates recycling of the copper importer CTR1 between plasma membrane and endocytic vesicles in HeLa cells (Curnock and Cullen, 2020). Compared to control cells, knockdown of VPS35 enhances survivability of cells in high copper that is suggestive of lower intracellular copper accumulation and hence lower copper-induced cytotoxicity. This is primarily due to regulation of CTR1 and not ATP7B (HeLa cells do not express ATP7B, Source: Human Protein Atlas and our data). In this study by Curnock and Cullen, the treatment was carried out for at least 48 hours and within a range of 3.125uM to 800uM copper. At 50uM copper, no significant difference of cell survivability and hence intracellular copper levels were observed between KO and control cells. This result suggests that the lower intracellular copper content that we observe in VPS35 KD compared to control cells is primarily due to continued export function of ATP7B arrested on the lysosomes.

In summary in this study we establish that, ATP7B traffics to active acid-hydrolase containing endolysosomes at high copper where it juxtaposes with VPS35 and contributes to the formation of a complex that comprises of at least ATP7B, VPS35 and VPS26 in addition to other proteins. Upon triggering the retrograde pathway by subsequent copper chelation, retromer regulates the recycling of ATP7B from the lysosome to the TGN (illustrated in Fig. 8).

## Discussion:

The copper transporting ATPase, ATP7B exports copper through lysosomes (Polishchuk et al., 2014). ATP7B (160kDa) is a large 8 membrane spanning protein with a total of 1465 residues. ATP7B resides on the TGN membrane at basal copper levels and traffics to

Lamp1 and Rab7 positive compartments at high copper. We argue that it would be highly wasteful for the cell to degrade ATP7B after each cycle of copper export from the TGN to the lysosomes. At the onset we determined that ATP7B primarily localizes on the active acid hydrolase positive endolysosomes at high copper. Since ATP7B is a recycling protein, we wondered whether ATP7B recycles back from these compartments after it pumps copper in the endolysosomal lumen for either export out of the cell or for reutilization as a nutrient that requires to be investigated. Interestingly, the protein does not get degraded unlike many other cargoes that are destined for degradation at the lysosomes. Rather, low pH in lysosomal lumen might help the release of copper from the His residues that are located between TM1-TM2 loop as shown in its homologue ATP7A (LeShane et al., 2010; Barry et al., 2011; Otoikhian et al., 2012) and binds copper.

Further we investigated the regulatory mechanism of retrograde trafficking of ATP7B. In a preliminary proteome analysis on GFP-ATP7B vesicles isolated from HepG2 cells (data not shown), we have identified members of the retromer complex. Previously (Harada et al., 2000) had shown that ATP7B resides in late endosome (Rab7 positive) in high copper. Retromer is recruited on endosomal membrane by sequential action of Rab5 and Rab7 (Rojas et al., 2008).

Before investigating the role of retromer in retrieval of ATP7B from lysosomes, we first determined if ATP7B is stable in lysosomal and Rab7 compartments. Similar to observations made by (Polishchuk et al., 2014) that even up to 200µM copper treatment in HepG2 cells, ATP7B shows no significant degradation, we noticed no change in its abundance at 250µM copper. At high copper ATP7B primarily localized at the active, hydrolase positive recycling endolysosomes with a smaller fraction at the terminal storage lysosomes. Interestingly, upon further elevating intracellular copper, though fraction of ATP7B stays unaltered at the active endolysosomes, an increase in its abundance was noticed in storage lysosomes. We argue that this shift of ATP7B's abundance equilibrium is due to a relay effect of ATP7B trafficking from TGN to active endolysosomes and finally to storage endolysosomes. At 250uM copper, further emptying of ATP7B from TGN is compensated with its increase at the storage terminal lysosome.

Upon examining triple-colocalization of ATP7B, VPS35 and Lamp1 in fixed cells, we notice that the level of overlap is moderate at high copper. This might be attributed to the fact that at a given point in copper treated cells, the nature of vesicles are highly heterogeneous comprising of retrograde and anterograde vesicles and that too at various stages of trafficking. We hypothesize that the endolysosomes would exhibit a higher co-residence of

VPS35 and ATP7B if we are able to synchronize the TGN exit (upon copper treatment) and endolysosomal exit (upon subsequent copper removal) of ATP7B. However, time lapse imaging showed that GFP-ATP7B and mCherry-Vps35 colocalizes in the compartment for a few minutes. In VPS35 kd cells, ATP7B is trapped in the endolysosomes even upon activating the retrograde pathway (Copper>BCS). We reason that ATP7B recycles back to TGN directly and not via plasma membrane as we did not observe ATP7B staining at the plasma membrane or even at the cortical actin (data not shown). This might be due to the non-polarized nature of the HepG2 cells used in this study.

Interestingly, using conventional biochemical assays, we did not detect any direct interaction of ATP7B and VPS35 (or VPS26). This is possibly due to the fact that though retromer complex regulates lysosomal exit of ATP7B, the interaction is mediated via a different member of the complex. This proposition is substantiated by co-detection of ATP7B, VPS35 and VPS26 in a supercomplex (>>250kDa) and also proximity of ATP7B and VPS35 at a range ≤40nm as detected in the PLA study. Our observation suggests that the retromer complex along with the WASH, the CCC complex consisting of COMMD1 and the Rab-GTPase, Rab7 co-ordinates the recycling of ATP7B from the endolysosomal compartments. However, the order of interaction of these complexes with the cargo is still to be determined.

Retromer complex shows heterogeneity in its subunits that are responsible for binding to the cargo (Belenkaya et al., 2008; Feinstein et al., 2011; Zhang et al., 2012; Follett et al., 2016; Suzuki et al., 2019; ). It has been shown that the canonical recycling signal for the Divalent Cation Transporter (DMT1-II) binding of retromer is mediated via the interface of VPS26 and SNX3 in a hybrid structural model shows that the α-solenoid fold extends the full length of Vps35, and that Vps26 and Vps29 are bound to its two opposite ends (Hierro et al., 2007; Lucas et al., 2016). This extended structure suggests that multiple binding sites for the SNX complex and receptor cargo are present. It has been shown show that membrane recruitment of retromer is mediated by recognition of SNX3 and RAB7A, by the VPS35 subunit. These bivalent interactions prime retromer to capture integral membrane cargo, which enhances membrane association of retromer and initiates cargo sorting (Zhao et al., 2007). Further studies are needed to be carried out to identify the exact interface of ATP7B-retromer interaction.

How copper (or copper removal) mediates triggering of ATP7B's retrograde pathway is not understood. It is likely that copper binding to the 6 MBD on ATP7B N-terminus, exposes

the upstream 1-63 N-terminal domain containing the $^{41}$NXXY$^{44}$ domain. However, role of C-terminus cannot be completely discounted as Braiterman et al has shown that multiple regulatory phosphorylation sites lie on the C-terminus that might play an indirect role in regulation of ATP7B trafficking by retromer complex (Braiterman et al., 2015). Additionally, ATP7B (and also ATP7A) harbors di-leucine motifs on the C-terminal that has been shown to be crucial in trafficking regulation and its retrieval to the TGN ( Petris et al., 1998; Francis et al., 1999; Jain et al., 2015).

Wilson disease, though a Mendelian disorder caused by mutations only in *ATP7B* gene, shows a large spectrum of symptoms and age of onset. We hypothesize that polymorphisms and mutations in trafficking regulatory proteins might be responsible for imparting such high phenotypic heterogeneity. Mutations and SNPs in the retromer subunit genes are associated with many hereditary conditions ( Small, 2008; Shannon et al., 2014; Reitz, 2017; Chen et al., 2017; Rahman and Morrison, 2019). Varadarajan et al, reported significant association of SNPs of retromer complex genes (SNX1, SNX3 and Rab7A) with Alzheimer's disease (Vardarajan et al., 2012). Similarly, VPS35 hemizygous condition accentuates Alzheimer's disease neuropathology (Wen et al., 2011). Additionally, Parkinson's disease-linked *D620N-VPS35* knocking mice manifest tau neuropathology and dopaminergic neurodegeneration (Chen et al., 2019). It would be important to extend the knowledge of role of retromers in ATP7B trafficking to delineate genotype-phenotype correlationship in Wilson disease patients.

## Materials and methods

### Plasmids and antibodies

GFP-ATP7B construct was available in lab. The mCherry WT-VPS35 and mCherry VPS35 (*R107A*) construct was a kind gift from Dr. Sunando Datta, IISER Bhopal, India. mCherry Rab7a-7 (Plasmid # 55127) was purchased from Addgene. mCherry Rab7a-7 T22N mutant was prepared following Q5® Site-Directed Mutagenesis Kit (# E0554) protocol. GFP- wtCOMMD1, T174M and K167/173E mutant constructs was kindly gifted by Dr. Jason Burkhead, Univ. of Alaska, Anchorage. Following are the antibodies that has been used for experiments: rabbit anti-ATP7B (# ab124973, Abcam), mouse anti-golgin97 (# A21270, Invitrogen ), goat anti-VPS35 (# NB 100-1397, Novus Biologicals), mouse anti-VPS26 (# NBP 236754, Novus Biologicals ), mouse anti-VPS35 (# sc-374372, Santa Cruz Biotechnology); for western blot, mouse anti-Lamp1 (DSHB: # H4A3), mouse anti-Rab7 (# sc-376362, Santa Cruz Biotechnology), Donkey anti-Rabbit IgG (H+L) Alexa Fluor 488 (# A-21206, Invitrogen ), Goat anti-Rabbit IgG (H+L) Alexa Fluor Plus 647 (# A32733, Invitrogen), Donkey anti-Mouse IgG (H+L) Alexa Fluor Plus 647 (# A32787, Invitrogen), Donkey anti-Goat IgG (H+L) Alexa Fluor 568 (# A-11057, Invitrogen), Donkey anti-Mouse IgG (H+L) Alexa Fluor 568 (# A10037, Invitrogen), mouse anti-Cation-independent mannose-6-phosphate receptor (DSHB: # 86f7), mouse anti-Lamp2 (DSHB: # H4B4), mouse anti-Na/K ATPase (ATP1A1 # MA3-929, Invitrogen), goat anti Rab11 (# sc-6565, Santa Cruz Biotechnology), mouse anti gamma-tubulin (# NB500-574, Novus Biologicals ), Rabbit anti GAPDH (# BB-AB0060, BioBharati ) and Rabbit anti gamma-actin. Sheep anti TGN46 was a kind gift from Prof. Carolyn Machamer, Johns Hopkins University. Endotoxin free plasmid isolation was done using EndoFree Plasmid Maxi Kit (Qiagen# 12362).

### Cell lines and cell culture

HepG2 cells were grown and maintained in complete medium containing low glucose Minimum Essential Medium (MEM) (# 41500-034, Thermo Fisher Scientific) supplemented with 10% Fetal Bovine Serum (# 10270-106, Thermo Fisher Scientific), 1X Penicillin-Streptomycin (# A001, HIMEDIA), 1X Amphotericin B (# 15290026, Thermo Fisher Scientific). Similarly HEK293Tcells were grown and maintained in Dulbecco's modified Eagle's medium (DMEM) (#CC3004.05L, Cellclone ) supplemented with 10% Fetal Bovine Serum, 1X Penicillin-Streptomycin, 1X Amphotericin B. For transfection of plasmids in HepG2 cell, Lipofectamine 3000 reagent (#L3000-001, Invitrogen) was used

according to manufacturer's protocol. For transfection in HEK293T, for live cell imaging, JetPrime (# 114-07, PolyplusTransfection) transfection reagent was used. Both cell lines were free of any contamination.

**Copper and BCS treatments**

For studying the trafficking or other biochemical assay of ATP7B in HepG2, copper chloride ($CuCl_2$) either in 50µM or 250 µM concentration was used. Similarly, Bathocuproine disulfonate (BCS), a copper chelator, was used either in 50µM or 250 µM concentration. Both the reagents were prepared fresh in autoclaved miliQ-water prior to treatment.

**Endocytic Uptake of Fluorescent Dextran**

Endocytic compartments in cultured HepG2 cells were loaded with 0.5 mg/ml lysine-fixable dextran-Alexa 647, from Thermo Fisher Scientific in culture medium for 4 hr at $37^0$C followed by incubation in conjugate-free medium for 20 hr as previously described (Bright et al., 1997).

**Incubation with Cathepsin B Substrate**

To label endocytic organelles in which cathepsin B was catalytically active, HepG2 cells were incubated with the Magic Red substrate from ImmunoChemistry Technologies, as per manufacturer's instruction.

**Knockdown assays**

Accell Human VPS35 (55737) siRNA-SMARTpool (#E-010894-00-0010), Accell Non-targeting siRNA (#D-001910-01-05), Accell siRNA Delivery Media (#B-005000-100), 5X siRNA Buffer (#B- 002000-UB-100) and Molecular Grade RNase-free water (#B-003000-WB-100) were purchased from Dharmacon. HepG2 cells were seeded in complete medium at a density of $1.5\times10^5$ cells/ml in coverslips heat fixed on 24-well plate. Cells were allowed to double for approx. 48hrs (doubling time of HepG2). After 48 hours, media was discarded, rinsed with 1X PBS pH 7.4 and si RNAs were added at a final concentration of 1µM resuspended in Accell siRNA Delivery Media (# B- 00-5000-100). This condition was maintained for 72 hours after which the si-RNA containing media was replaced with complete media and again maintained for another 24 hours. This ensures better knock

down at protein level. To validate knock down of VPS35, western blot was performed following same protocol from one well of 24 well plate.

Lentiviral shRNA RNAi Consortium (TRC) protocol was used to produce TRC VPS35 lentiviral constructs (TRC VPS35 shRNA components (Dharmacon): RHS3979201863202, RHS3979201863553, RHS3979-201866801, RHS3979-201869452, RHS3979-201877513) (# RHS4533-EG55737) and TRC Lentiviral pLKO.1 stuffer control (# RHS4080). Knock down of VPS35 was validated by western blot.

**Immunofluorescence**

HepG2 cells were seeded at a density of (0.8-1.6×$10^5$ cells/ml) on coverslips heat fixed on wells of 24 well plate each time while conducting immunofluorescence. Any treatment was performed at a confluency of (60-70) %, including transfection. 4% Para-formaldehyde (PFA) fixation was done following treatment. After fixation cells were permeablized with chilled methanol and finally washed with 1X PBS. Fixation and permeablisation was carried out in cold condition. Cells were blocked in 3% BSA suspended in 1X PBS for either 2hours at room temperature (RT) or O/N at 4$^o$C. Following this, primary antibody ($1^0$) incubation was done at RT in moist chamber for 2hours. After 10 incubation, cells were washed with 1X PBST for 3 times and again re-incubated with corresponding secondary antibodies ($2^0$) for 1.3 hours at RT. This was followed by further washing with 1X PBST for 3 times and finally with 1X PBS for two times. Coverslips were fixed on glass slides using SIGMA Fluoroshield™ with DAPI mountant. (#F6057). The solvent for antibody suspension was 1% BSA in 1X PBST.

For STED sample preparation, HepG2 cells were seeded on glass coverslips, treated with copper (as mentioned in Fig. 6E). Treatment was done at 70% confluency. Cell were fixed with 2% PFA for 20mins followed by washing with 1X PBS, pH 7.2 for 15mins (× 2) and then quenched with 50mM $NH_4Cl$. Blocking and permeation was done for 30mins with 1% BSA along with 0.075% saponin. Cell were co-incubated with primary rabbit anti-ATP7B and goat anti-VPS35 for 2hrs at room temp. Followed by 1X PBS washing and incubation with secondary anti- rabbit Alexa 488 and anti-goat Alexa 647. Coverslips was mounted with ProLong™ Diamond Antifade Mountant with DAPI (# P36962).

**Time-lapse fluorescence microscopy**

HEK293T cells were seeded on confocal dishes (SPL) and were co-transfected separately with GFP-ATP7B and mCherry-VPS35-WT, mCherry-VPS35-Mutant (R107A) (gift by Sunando Datta, IISER Bhopal), using jetPRIME (Polyplus) transfecting regent as per

manufacturer protocol. Images were acquired using Leica SP8 confocal setup with 63x oil objective. For ATP7B & VPS35-WT/MT, images were taken at every 1.964 s interval using Lightning by Leica. For triple color time lapse fluorescence microscopy of ATP7B (green), DexA (blue) and Magic Red (red), GFP-ATP7B was transfected in HepG2 cell in confocal dish pre-incubated with DexA and Magic Red. Each image was captured at an interval of 5s for a total duration of 15mins. All time-lapse images were recorded in DMEM media without phenol red supplemented with 5% fetal bovine serum and 5mM HEPES. All the images were processed using Fiji and LASX software provided by Leica and videos were processed using Cyberlink Powerdirector.

**Microscopy**

All images were acquired with Leica SP8 confocal platform using oil immersion 63X objective and deconvoluted using Leica Lightning software. For Structured Illumination Microscopy, images acquisition was taken at 100X magnification in Zeiss Elyra PSI. For Stimulated emission depletion (STED) microscopy, imaging was done in Leica STED 3X. For Alexa 647, 775 STED laser line was used and for Alexa 488, 592 laser line was used for depletion. Line average was set at 4 and pixel size was kept as 25nm to achieve maximum resolution. STED corrected images were deconvoluted and processed by Scientific Volume Imaging of Huygens Professional Software with default settings.

**Immunoblotting**

HepG2 cells were grown on 60mm dish and cell pellet was collected at 70% confluency. For lysate preparation of membrane protein dry pellet was dissolved in 200µL of lysis buffer (composition: sucrose 250mM, EDTA 1mM, EGTA 1mM, 1X PBS as solvent, 1X protease cocktail inhibitor) and incubated on ice for 1hour with intermittent tapping. Dounce homogenization of dissolved pellet was done for approx. 400 times followed by syringe up down with 22-24 gauge needle for 20-25 times on ice. This enables the cell to rupture completely. The soup was centrifuged at 600 R.C.F at $4^0$C for 10mins to discard debris and nucleus. Further mitochondrial fraction was discarded by centrifugation at 3000 R.C.F for 10mins at $4^0$C. The resultant soup was subjected for ultra-centrifugation at 1,00,000 R.C.F for 1hour at $4^0$C to collect membrane fraction. Pellet was dissolved in membrane solubilizing buffer (composition: sucrose 250mM, EDTA 1mM, EGTA 1mM, NP-40 1.0%, Triton X-100 1.0%, 1X PBS as solvent, 1X protease cocktail inhibitor). For, soluble protein, whole cell lysate was prepared with RIPA lysis buffer (composition: 10mM Tris-Cl pH 8.0, 1mM EDTA, 0.5mM EGTA, 1.0% Triton X-100, 0.1% sodium deoxycholate,

0.1% sodium dodecyl sulphate, 140mM NaCl, 1X protease cocktail inhibitor). Dry pellet was dissolved in RIPA lysis buffer and incubated on ice for 30mins with intermittent tapping. The solution is then sonicated with a probe sonicator (3-4 pulses, 5sec, and 100mA). Followed by this, centrifugation at 20,000 R.P.M for 20mins at $4^0$C was done to pellet down cellular insoluble debris and soup was collected. Protein estimation was carried out with Bradford reagent (# B6916-500ML, Sigma-Aldrich) following manufacturer's protocol. Protein sample preparation was done by adding 4X loading buffer (composition: Tris-Cl pH 6.81, 4% SDS, 10% β-ME, 20% glycerol, 0.02% bromophenol blue, urea 8M) to a final concentration of 1X and ran on SDS PAGE (6% for membrane fraction and 10-12% for soluble fraction) to separate proteins according to molecular mass. This was further followed by wet transfer of proteins onto nitrocellulose membrane (1620112, BioRad). After transfer, the membrane was blocked with 3% BSA in 1X Tris-buffered saline (TBS) buffer pH7.5 for 2hrs at RT with mild shaking. Primary antibody incubation was done overnight at 40 C following blocking and then washed with 1X TBST (0.01% Tween-20) for 10mins (× 3 times). HRP conjugated respective secondary incubation was done for 1.3 hrs at RT, further washed and signal was developed by ECL developer (170-5060, BioRad/ 1705062, BioRad) in chemiluminescence by Chemi Doc (BioRad).

**Co-immunoprecipitation:**

All solutions were pre-chilled to 4°C and all steps were carried out on ice. HEK293T cells were transfected with GFP-ATP7B and treated with different Cu conditions followed by washing with 1x PBS and lysis using lysis buffer (10mM Tris-Cl pH 7.5, 150mM NaCl, 0.5mM EDTA, 0.5 % NP40, PMSF and protease inhibitor cocktail in ddH2O). Cell extracts were triturated with 2ml syringe and incubated for total 45minutes and the insoluble materials were sedimented at 16,000g for 10 min at 4°C. Co-IP experiment was performed using GFP- trap beads (ChromoTek, # gta-20) following the manufacturer protocol. The supernatants were diluted using diluted buffer (10mM Tris-Cl pH 7.5, 150mM NaCl, 0.5mM EDTA, PMSF and protease inhibitor cocktail in ddH2O to yield 0.25 % NP40) and incubated with GFP-trap beads for 2hr at 4°C on a rotating wheel. Finally the interacting proteins were eluted using 0.2M glycine and used for western blotting. Western blotting of VPS35, VPS26 and GFP: Samples for Western blotting were resolved by SDS- PAGE and separated proteins were transferred to nitrocellulose membrane. After protein transfer, the membrane was blocked in 5% non-fat milk powder (for VPS35&VPS26) and 3% BSA (for GFP) and incubated with primary antibody diluted in 5% non-fat milk powder (for mouse

anti-VPS35 & mouse anti-VPS26 1:1500 dilution) or 1%BSA (for rabbit anti-GFP 1:10000 dilution) overnight at 4°C. Following incubation, the membrane was briefly washed three times with TBS-T and incubated with HRP-conjugated secondary antibodies (anti-mouse HRP 1:5000 dilution and anti-rabbit HRP 1:15000 dilution) diluted in 5% non-fat milk powder or 1%BSA for 1.5hr at RT. The membrane was washed three times for 5 min in TBS-T flowed by two times washing with TBS at RT and incubated for 5min at RT with Enhanced Chemiluminescence (ECL) substrate and ECL plus (1:1).

**In-vivo metabolic labelling and UV crosslinking**

HEK293T cell was transfected with GFP-ATP7B and supplemented with modified DMEM-LM (# 30030, Sigma-Aldrich) media (without leucine and methionine) and photo Leucine (# 22610, Thermo Scientific) and photo Methionine (# 22615, Thermo Scientific). Cell was treated with either 100µM $CuCl_2$ or 50µM BCS for 4hrs and subjected to UV crosslinking at 365nm for 15mins. Cell was processed for co-immunoprecipitation (Co-IP) assay following GFP-Trap_A (code- gta-20) Chrormotek as described above with few modifications. All steps were carried out on ice. Briefly, cell lysis was done with Co-IP compatible 200 µl lysis buffer (10 mM Tris/Cl pH 7.5, 150 mM NaCl, 0.5 mM EDTA, 0.5 % Nonidet™ P40, 1X protease cocktail inhibitor and 1mM PMSF). Trituration was done with 26 gauge needle in 1ml syringe for approx. 40times for cell to completely lyse followed by centrifugation at 3000g for 5mins at 40C. The sup was collected and diluted with 300 µl of dilution buffer (10 mM Tris/Cl pH 7.5, 150 mM NaCl, 0.5 mM EDTA). GFP-Trap A beads slurry was equilibrated with dilution buffer and incubated with the diluted supernatant and subjected to tumbling end-over on a rotatory wheel at 10rpm for 4hrs (first two hours at room temperature and the next two hours at $4^0$C).

**Proximity ligation assay**

Proximity ligation assay was performed according to manufacturer's protocol (Duolink™ PLA Technology, Sigma). Briefly, HepG2 cell was grown on glass coverslips upto 70% confluency and treated with copper for 2hrs, fixed with 4% paraformaldehyde and permeabilized with 0.1% saponin. Thereafter, cell was blocked with blocking solution (DUO82007) for 1hr at 370C and incubated with primary antibodies for 2hrs at 370C followed by washing twice with Wash Buffer A (DUO82049-4L) for 5mins on gentle orbital shaker at room temperature (RT). During washing, the secondary PLA probes (DUO92005, DUO92003, DUO92001) were diluted to 1:5 with antibody diluent (DUO82008) and cell was incubated with it for 1hr at 370C. Cell was further washed in

same way. During washing, the ligation mixture was prepared by diluting the ligase enzyme (DUO82029) 1:40 in 1X ligation buffer (DUO82009) and applied onto cell. It was then incubated for 30mins at 370C followed by washing twice in Wash buffer A for 2mins at RT. During washing, the amplification mixture was prepared by diluting the polymerase enzyme (DUO82030) 1:80 in 1X amplification buffer (DUO82010) and applied on cell with incubation at 370C for 100mins. After incubation, cell was washed twice with Wash Buffer B for 10mins. A final wash with 0.01X Wash buffer B was given prior mounting with DAPI containing mountant. Images was acquired with Leica SP8 confocal platform using 576 nm (Cy3) filter.

**Cell Viability test using Neutral Red assay**

*Neutral Red assay:* Cell cytotoxicity to copper in the background of VPS35 knockdown in cultured HepG2 cell was determined by Neutral Red assay. Briefly, $6 \times 10^3$ viable cells were seeded in each well of a 96-well microplate (Nunc) and incubated at 37 °C (5% $CO_2$ atmosphere). After24 hrs of incubation, the medium was replaced with a fresh one containing lentiviral sh_RNA (scrambled and pooled VPS35). After 48 hrs of incubation, the medium was replaced with a fresh one containing the desired concentration copper (0µM and 50µM) where each concentration was loaded in quadruplicate. After 24 hrs of incubation with the copper solution, the medium was removed and a fresh medium was added with neutral red (# N7005, Sigma-Aldrich) at a final concentration of 40µg/ml and incubated for 2hrs. This was followed by washing with destaining solution (50% EtOH, 1% Acetic acid, 49% MiliQ water). The absorbance was recorded at 540 nm using SYNERGY H1 microplate reader, Biotek and percentage of viable cells was calculated against copper concentrations. Each condition had four replicates ($p<0.1$). Data was plotted in *GraphPad Prism 8* to obtain the histogram normalized against corresponding scrambled controls. Non-parametric t-test performed to obtain p-value.

**Determination of the cellular copper concentration in VPS35 Knockdown cell**

The HepG2 cells were seeded in 35 mm Petri dish at 37 °C (5% $CO_2$ atmosphere). After24 hrs of incubation, the medium was replaced with a fresh one containing lentiviral sh_RNA (scrambled and pooled VPS35). After 48 hrs of incubation, the medium was replaced with a fresh one containing the desired concentration copper (0µM and 50µM) and incubated for 2hrs. Cells was washed with 1X dPBS for several times and pelleted down. Dry pellet was weighed which was ≈ 0.25mg. For each sample, 2 mL 65% suprapur $HNO_3$ + 4 mL

deionised water added prior to digestion for 1 h. (MWD conditions: Power=800 W; Temperature=100℃; Hold time= 1 h). After digestion, samples were syringe filtered through 0.45 micron filter. Cu calibration done by acid digestion of Cu foil (procured from Alfa Aeasar) in 10 mL suprapur HNO3 for 1 h. (MWD conditions: Power=400 W; Temperature=100℃; Hold time= 1 h). From the obtained solution, different strengths of Cu in ppb were prepared and used for calibration. Similar acid digestion steps were followed for samples in microwave digester. This solution was used to determine the cellular copper concentrations using a Thermo Scientific *Inductively coupled plasma optical emission spectroscopy* (ICP-OES) iCAP 6500. For each sample, a total of five replicates were used to calculate the average intracellular copper concentration ($p<0.1$).

**Cell count and vesicle count for data analysis**

Number of Cells considered for analysis has been mentioned in bar plots in figures as 'n'. For Fig.6A to assess colocalization between ATP7B, VPS35 and Lamp1, a total of 12 cells were taken to calculate ATP7B and VPS35 signals that are colocalizing together in Lamp1 positive compartments in high copper. 88 ATP7B (green) puncta were considered as actual signals. This served as reference to calculate relative abundance of green (ATP7B), cyan (VPS35), red (Lamp1) signals that are clustered together. 37 such triple coloured clusters were obtained.

**Image analysis and statistics**

Images were analyzed in batches using ImageJ (Schneider et al., 2012), image analysis software. For colocalization study, Colocalization_Finder plugin was used. RO Is were drawn manually on best z-stack for each cell. For three protein colocalization study, the other two protein co-residing vesicles were isolated using Analyze Particle tool, and colocalization study were carried on with the reference protein, ATP7B in our case. To calculate the lysosomal distribution of ATP7B, fractions of ATP7B localized in MR and Dextran positive endosomes were obtained using Mender's colocalization coefficient (MCC) (Manders et al., 1993) Merged image of MR channel and Dextran channel was obtained in greyscale which was used to obtain the total lysosomal ATP7B, Using set theory formulae: $|A \cap B| = |A| + |B| - |A \cup B|$, the rest were deducted. RGB_Profiler plugin was used to obtain the line profile graph. For statistical analysis and plotting, ggplot2 (*Hadley Wickham Ggplot2 SPIN*, 2009) package was used in R v-3.4.0 (*R: A Language and Environment for Statistical Computing*, 2015). Non-parametric tests for unpaired

datasets (Kruskal Wallis test and Mann-Whitney U test) were performed for all the samples.

**Acknowledgments**

This work was supported by DBT-Wellcome Trust India Alliance Fellowship (IA/I/16/1/502369) and Early Career Research Award (ECR/2015/000220) from SERB, Department of Science and Technology (DST), Government of India and IISER K intramural funding to AG. SM and IB was supported by Pre-doctoral fellowship from Council of Scientific and Industrial Research, India. TS was supported by National Postdoctoral Fellowship, SERB, India. We thank Dr. Ashima Bhattacharjee for critical review of the manuscript.

Author contributions: AG and SD designed the experiments and wrote the manuscript. SD, Ruturaj, IB, NS and TS did the experiments and analyzed the data. SM wrote the codes and analysed the data. Ruturaj helped with time-lapse imaging. Dr. Anupam Banerjee (Zeiss) helped us with SIM imaging at JNCASR. STED microscopy was carried out at the Leica microscopy facility at IISER Pune. All authors reviewed the results and approved the final version of the manuscript.

We thank Prof. Arindam Mukherjee (IISER Kolkata), Dr. Oishee Chakrabarti and Prof. Susanta Lahiri (Saha Institute of Nuclear Physics), Dr. Ashima Bhattacharjee (Amity Univ. Kolkata), Dr. Sunando Datta, (IISER Bhopal), Dr. Jason Burkhead, (Univ. of Alaska) and Dr. Partho Sarothi Ray (IISER Kolkata) for sharing their reagents, constructs and instruments with us.

The authors declare no competing financial interests.

## Bibliography


**Abdelghaffar, T. Y., Elsayed, S. M., Elsobky, E., Bochow, B., Büttner, J. and Schmidt, H.** (2008). Mutational analysis of ATP7B gene in Egyptian children with Wilson disease: 12 Novel mutations. *J. Hum. Genet.* **53**, 681–687.

**Abu-Remaileh, M., Wyant, G. A., Kim, C., Laqtom, N. N., Abbasi, M., Chan, S. H., Freinkman, E. and Sabatini, D. M.** (2017). Lysosomal metabolomics reveals V-ATPase- and mTOR-dependent regulation of amino acid efflux from lysosomes. *Science (80-. ).* **358**, 807–813.

**Aggarwal, A., Chandhok, G., Todorov, T., Parekh, S., Tilve, S., Zibert, A., Bhatt, M. and Schmidt, H. H. J.** (2013). Wilson disease mutation pattern with genotype-phenotype correlations from Western India: Confirmation of p.C271* as a common indian mutation and identification of 14 novel mutations. *Ann. Hum. Genet.* **77**, 299–307.

**Ala, A., Aliu, E. and Schilsky, M. L.** (2015). Prospective Pilot Study of a Single Daily Dosage of Trientine for the Treatment of Wilson Disease. *Dig. Dis. Sci.* **60**, 1433–1439.

**Arighi, C. N., Harmell, L. M., Aguilar, R. C., Haft, C. R. and Bonifacino, J. S.** (2004). Role of the mammalian retromer in sorting of the cation-independent mannose 6-phosphate receptor. *J. Cell Biol.* **165**, 123–133.

**Barry, A. N., Otoikhian, A., Bhatt, S., Shinde, U., Tsivkovskii, R., Blackburn, N. J. and Lutsenko, S.** (2011). The lumenal loop Met 672-Pro 707 of copper-transporting ATPase ATP7A binds metals and facilitates copper release from the intramembrane sites. *J. Biol. Chem.* **286**, 26585–26594.

**Belenkaya, T. Y., Wu, Y., Tang, X., Zhou, B., Cheng, L., Sharma, Y. V., Yan, D., Selva, E. M. and Lin, X.** (2008). The Retromer Complex Influences Wnt Secretion by Recycling Wntless from Endosomes to the Trans-Golgi Network. *Dev. Cell* **14**, 120–131.

**Blaby-Haas, C. E. and Merchant, S. S.** (2014). Lysosome-related organelles as mediators of metal homeostasis. *J. Biol. Chem.* **289**, 28129–28136.

**Braiterman, L., Nyasae, L., Guo, Y., Bustos, R., Lutsenko, S. and Hubbard, A.** (2009). Apical targeting and Golgi retention signals reside within a 9-amino acid sequence in the copper-ATPase, ATP7B. *Am. J. Physiol. - Gastrointest. Liver Physiol.* **296**,.

**Braiterman, L. T., Murthy, A., Jayakanthan, S., Nyasae, L., Tzeng, E., Gromadzka, G., Woolf, T. B., Lutsenko, S. and Hubbard, A. L.** (2014). Distinct phenotype of a Wilson disease mutation reveals a novel trafficking determinant in the copper transporter ATP7B. *Proc. Natl. Acad. Sci. U. S. A.* **111**,.

**Braiterman, L. T., Gupta, A., Chaerkady, R., Cole, R. N. and Hubbard, A. L.** (2015). Communication between the N and C termini is required for copper-stimulated Ser/Thr phosphorylation of Cu(I)-ATPase. *J. Biol. Chem.* **290**, 8803–8819.

**Bright, N. A., Reaves, B. J., Mullock, B. M. and Luzio, J. P.** (1997). Dense core lysosomes can fuse with late endosomes and are re-formed from the resultant hybrid organelles. *J. Cell Sci.*

**Bright, N. A., Davis, L. J. and Luzio, J. P.** (2016). Endolysosomes Are the Principal Intracellular Sites of Acid Hydrolase Activity. *Curr. Biol.* **26**, 2233–2245.

**Burd, C. and Cullen, P. J.** (2014). Retromer: A master conductor of endosome sorting. *Cold Spring Harb. Perspect. Biol.* **6**,.

**Burkhead, J. L., Morgan, C. T., Shinde, U., Haddock, G. and Lutsenko, S.** (2009). COMMD1 forms oligomeric complexes targeted to the endocytic membranes via specific interactions with phosphatidylinositol 4,5-Bisphosphate. *J. Biol. Chem.*

**Caca, K., Ferenci, P., Jurgen Kuhn, H., Polli, C., Willgerodt, H., Kunath, B., Hermann, W., Mossner, J. and Berr, F.** (2001). High prevalence of the h1069q mutation in east german patients with wilson disease: Rapid detection of mutations by limited sequencing and phenotype-genotype analysis. *J. Hepatol.* **35**, 575–581.

**Canuel, M., Lefrancois, S., Zeng, J. and Morales, C. R.** (2008). AP-1 and retromer play opposite roles in the trafficking of sortilin between the Golgi apparatus and the lysosomes. *Biochem. Biophys. Res. Commun.* **366**, 724–730.

**Chen, Y. F., Chang, Y. Y., Lan, M. Y., Chen, P. L. and Lin, C. H.** (2017). Identification of VPS35 p.D620N mutation-related Parkinson's disease in a Taiwanese family with successful bilateral subthalamic nucleus deep brain stimulation: A case report and literature review. *BMC Neurol.* **17**,.

**Chen, X., Kordich, J. K., Williams, E. T., Levine, N., Cole-Strauss, A., Marshall, L., Labrie, V., Ma, J., Lipton, J. W. and Moore, D. J.** (2019). Parkinson's disease-linked D620N VPS35 knockin mice manifest tau neuropathology and dopaminergic neurodegeneration. *Proc. Natl. Acad. Sci. U. S. A.* **116**, 5765–5774.

**Cheng, X. T., Xie, Y. X., Zhou, B., Huang, N., Farfel-Becker, T. and Sheng, Z. H.** (2018). Characterization of LAMP1-labeled nondegradative lysosomal and endocytic compartments in neurons. *J. Cell Biol.* **217**, 3127–3139.

**Cox, D. W., Prat, L., Walshe, J. M., Heathcote, J. and Gaffney, D.** (2005). Twenty-four novel mutations in Wilson disease patients of predominantly European ancestry. *Hum. Mutat.*

**Cui, Y., Carosi, J. M., Yang, Z., Ariotti, N., Kerr, M. C., Parton, R. G., Sargeant, T. J. and Teasdale, R. D.** (2019). Retromer has a selective function in cargo sorting via endosome transport carriers. *J. Cell Biol.* **218**, 615–631.

**Curnock, R. and Cullen, P. J.** (2020). Mammalian copper homeostasis requires retromer-dependent recycling of the high-affinity copper transporter 1. *J. Cell Sci.* **133**,.

**Deatherage, C. L., Nikolaus, J., Karatekin, E. and Burd, C. G.** (2020). Retromer forms low order oligomers on supported lipid bilayers. *J. Biol. Chem.*

**Fahrni, C. J.** (2013). Synthetic fluorescent probes for monovalent copper. *Curr. Opin. Chem. Biol.* **17**, 656–662.

**Feinstein, T. N., Wehbi, V. L., Ardura, J. A., Wheeler, D. S., Ferrandon, S., Gardella, T. J. and Vilardaga, J. P.** (2011). Retromer terminates the generation of cAMP by internalized PTH receptors. *Nat. Chem. Biol.* **7**, 278–284.

**Follett, J., Bugarcic, A., Yang, Z., Ariotti, N., Norwood, S. J., Collins, B. M., Parton, R. G. and Teasdale, R. D.** (2016). Parkinson disease-linked Vps35 R524W mutation impairs the endosomal association of retromer and induces α-synuclein aggregation. *J. Biol. Chem.* **291**, 18283–18298.

**Forbes, J. R. and Cox, D. W.** (1998). Functional characterization of missense mutations in ATP7B: Wilson disease mutation or normal variant? *Am. J. Hum. Genet.*

**Francis, M. J., Jones, E. E., Levy, E. R., Martin, R. L., Ponnambalam, S. and Monaco, A. P.** (1999). Identification of a di-leucine motif within the C terminus domain of the Menkes disease protein that mediates endocytosis from the plasma membrane. *J. Cell Sci.*

**Fuse, A., Furuya, N., Kakuta, S., Inose, A., Sato, M., Koike, M., Saiki, S. and Hattori, N.** (2015). VPS29-VPS35 intermediate of retromer is stable and may be involved in the retromer complex assembly process. *FEBS Lett.* **589**, 1430–1436.

**Gershlick, D. C. and Lucas, M.** (2017). Endosomal Trafficking: Retromer and Retriever Are Relatives in Recycling. *Curr. Biol.* **27**, R1233–R1236.

**Gokool, S., Tattersall, D., Reddy, J. V. and Seaman, M. N. J.** (2007). Identification of a conserved motif required for Vps35p/Vps26p interaction and assembly of the retromer complex. *Biochem. J.* **408**, 287–295.

**Guha, A., Ahuja, D., Das Mandal, S., Parasar, B., Deyasi, K., Roy, D., Sharma, V., Willard, B., Ghosh, A. and Ray, P. S.** (2019). Integrated Regulation of HuR by Translation Repression and Protein Degradation Determines Pulsatile Expression of p53 Under DNA Damage. *iScience* **15**, 342–359.

**Gupta, A. and Lutsenko, S.** (2009). Human copper transporters: Mechanism, role in human diseases and therapeutic potential. *Future Med. Chem.* **1**, 1125–1142.

**Gupta, A., Aikath, D., Neogi, R., Datta, S., Basu, K., Maity, B., Trivedi, R., Ray, J., Das, S. K., Gangopadhyay, P. K., et al.** (2005). Molecular pathogenesis of Wilson disease: haplotype analysis, detection of prevalent mutations and genotype-phenotype correlation in Indian patients. *Hum. Genet.* **118**, 49–57.

**Gupta, A., Chattopadhyay, I., Mukherjee, S., Sengupta, M., Das, S. K. and Ray, K.** (2010). A novel COMMD1 mutation Thr174Met associated with elevated urinary copper and signs of enhanced apoptotic cell death in a Wilson Disease patient. *Behav. Brain Funct.* **6**,.

**Gupta, A., Bhattacharjee, A., Dmitriev, O. Y., Nokhrin, S., Braiterman, L., Hubbard, A. L. and Lutsenko, S.** (2011). Cellular copper levels determine the phenotype of the Arg875 variant of ATP7B/Wilson disease protein. *Proc. Natl. Acad. Sci. U. S. A.* **108**, 5390–5395.

**Gupta, A., Schell, M. J., Bhattacharjee, A., Lutsenko, S. and Hubbard, A. L.** (2016). Myosin Vb mediates Cu+ export in polarized hepatocytes. *J. Cell Sci.* **129**, 1179–1189.

**Gupta, A., Das, S. and Ray, K.** (2018). A glimpse into the regulation of the Wilson disease protein, ATP7B, sheds light on the complexity of mammalian apical trafficking pathways. *Metallomics* **10**, 378–387.

**Hadley Wickham ggplot2 SPIN**.

**Harada, M., Sakisaka, S., Kawaguchi, T., Kimura, R., Taniguchi, E., Koga, H., Hanada, S., Baba, S., Furuta, K., Kumashiro, R., et al.** (2000). Copper does not alter the intracellular distribution of ATP7B, a copper-transporting ATPase. *Biochem. Biophys. Res. Commun.* **275**, 871–876.

**Harrison, M. S., Hung, C. S., Liu, T. T., Christiano, R., Walther, T. C. and Burd, C. G.** (2014). A mechanism for retromer endosomal coat complex assembly with cargo. *Proc. Natl. Acad. Sci. U. S. A.*

**Hierro, A., Rojas, A. L., Rojas, R., Murthy, N., Effantin, G., Kajava, A. V., Steven, A. C., Bonifacino, J. S. and Hurley, J. H.** (2007). Functional architecture of the retromer cargo-recognition complex. *Nature* **449**, 1063–1067.

**Humphries, W. H., Szymanski, C. J. and Payne, C. K.** (2011). Endo-lysosomal vesicles positive for rab7 and lamp1 are terminal vesicles for the transport of dextran. *PLoS One* **6**,.

**Huster, D. and Lutsenko, S.** (2007). Wilson disease: Not just a copper disorder. Analysis of a Wilson disease model demonstrates the link between copper and lipid metabolism. *Mol. Biosyst.* **3**, 816–824.

**Jain, S., Farías, G. G. and Bonifacino, J. S.** (2015). Polarized sorting of the copper transporter ATP7B in neurons mediated by recognition of a dileucine signal by AP-1. *Mol. Biol. Cell* **26**, 218–228.

**Kambe, T.** (2011). An overview of a wide range of functions of ZnT and Zip Zinc transporters in the secretory pathway. *Biosci. Biotechnol. Biochem.* **75**, 1036–1043.

**Korolchuk, V. I. and Rubinsztein, D. C.** (2011). Regulation of autophagy by lysosomal positioning. *Autophagy* **7**, 927–928.

**Kurz, T., Eaton, J. W. and Brunk, U. T.** (2011). The role of lysosomes in iron metabolism and recycling. *Int. J. Biochem. Cell Biol.* **43**, 1686–1697.

**LeShane, E. S., Shinde, U., Walker, J. M., Barry, A. N., Blackburn, N. J., Ralle, M. and Lutsenko, S.** (2010). Interactions between copper-binding sites determine the redox status and conformation of the regulatory N-terminal domain of ATP7B. *J. Biol. Chem.* **285**, 6327–6336.

**Lucas, M., Gershlick, D. C., Vidaurrazaga, A., Rojas, A. L., Bonifacino, J. S. and Hierro, A.** (2016). Structural Mechanism for Cargo Recognition by the Retromer Complex. *Cell* **167**, 1623-1635.e14.

**Lutsenko, S.** (2016). Copper trafficking to the secretory pathway. *Metallomics* **8**, 840–852.

**Ma, M. and Burd, C. G.** (2020). Retrograde trafficking and plasma membrane recycling pathways of the budding yeast Saccharomyces cerevisiae. *Traffic*.

**MANDERS, E. M. M., VERBEEK, F. J. and ATEN, J. A.** (1993). Measurement of co-localization of objects in dual-colour confocal images. *J. Microsc.* **169**, 375–382.

**Materia, S., Cater, M. A., Klomp, L. W. J., Mercer, J. F. B. and La Fontaine, S.** (2012). Clusterin and COMMD1 independently regulate degradation of the mammalian copper ATPases ATP7A and ATP7B. *J. Biol. Chem.* **287**, 2485–2499.

**Mellado, M., Cuartero, Y., Brugada, R. and Verges, M.** (2014). Subcellular localisation of retromer in post-endocytic pathways of polarised Madin-Darby canine kidney cells. *Biol. Cell* **106**, 377–393.

**Miyayama, T., Hiraoka, D., Kawaji, F., Nakamura, E., Suzuki, N. and Ogra, Y.** (2010). Roles of COMM-domain-containing 1 in stability and recruitment of the copper-transporting ATPase in a mouse hepatoma cell line. *Biochem. J.* **429**, 53–61.

**Muchenditsi, A., Yang, H., Hamilton, J. P., Koganti, L., Housseau, F., Aronov, L., Fan, H., Pierson, H., Bhattacharjee, A., Murphy, R., et al.** (2017). Targeted inactivation of copper transporter Atp7b in hepatocytes causes liver steatosis and obesity in mice. *Am. J. Physiol. - Gastrointest. Liver Physiol.* **313**, G39–G49.

**Otoikhian, A., Barry, A. N., Mayfield, M., Nilges, M., Huang, Y., Lutsenko, S. and Blackburn, N. J.** (2012). Lumenal loop M672-P707 of the menkes protein (ATP7A) transfers copper to peptidylglycine monooxygenase. *J. Am. Chem. Soc.* **134**, 10458–10468.

**Petris, M. J., Camakaris, J., Greenough, M., LaFontaine, S. and Mercer, J. F. B.** (1998). A C-terminal di-leucine is required for localization of the Menkes protein in the trans-Golgi network. *Hum. Mol. Genet.* **7**, 2063–2071.

**Phillips-Krawczak, C. A., Singla, A., Starokadomskyy, P., Deng, Z., Osborne, D. G., Li, H., Dick, C. J., Gomez, T. S., Koenecke, M., Zhang, J. S., et al.** (2015). COMMD1 is linked to the WASH complex and regulates endosomal trafficking of the copper transporter ATP7A. *Mol. Biol. Cell* **26**, 91–103.

**Polishchuk, E. V., Concilli, M., Iacobacci, S., Chesi, G., Pastore, N., Piccolo, P., Paladino, S., Baldantoni, D., vanIJzendoorn, S. C. D., Chan, J., et al.** (2014). Wilson Disease Protein ATP7B Utilizes Lysosomal Exocytosis to Maintain Copper Homeostasis. *Dev. Cell* **29**, 686–700.

**R: A Language and Environment for Statistical Computing**.

**Rabanal-Ruiz, Y. and Korolchuk, V. I.** (2018). mTORC1 and nutrient homeostasis: The central role of the lysosome. *Int. J. Mol. Sci.* **19**,.

**Rahman, A. A. and Morrison, B. E.** (2019). Contributions of VPS35 Mutations to Parkinson's Disease. *Neuroscience* **401**, 1–10.

**Reitz, C.** (2017). Retromer Dysfunction and Neurodegenerative Disease. *Curr. Genomics* **19**, 279–288.

**Roelofsen, H., Wolters, H., Van Luyn, M. J. A., Miura, N., Kuipers, F. and Vonk, R. J.** (2000). Copper-induced apical trafficking of ATP7B in polarized hepatoma cells provides a mechanism for biliary copper excretion. *Gastroenterology* **119**, 782–793.

**Rojas, R., Van Vlijmen, T., Mardones, G. A., Prabhu, Y., Rojas, A. L., Mohammed, S., Heck, A. J. R., Raposo, G., Van Der Sluijs, P. and Bonifacino, J. S.** (2008). Regulation of retromer recruitment to endosomes by sequential action of Rab5 and Rab7. *J. Cell Biol.* **183**, 513–526.

**Schneider, C. A., Rasband, W. S. and Eliceiri, K. W.** (2012). NIH Image to ImageJ: 25 years of image analysis. *Nat. Methods* **9**, 671–675.

**Seaman, M. N. J.** (2004). Cargo-selective endosomal sorting for retrieval to the Golgi requires retromer. *J. Cell Biol.* **165**, 111–122.

**Seaman, M. N. J.** (2007). Identification of a novel conserved sorting motif required for retromer-mediated endosome-to-TGN retrieval. *J. Cell Sci.* **120**, 2378–2389.

**Seaman, M. N. J.** (2018). Retromer and Its Role in Regulating Signaling at Endosomes. *Prog. Mol. Subcell. Biol.* **57**, 137–149.

**Seaman, M. N. and Freeman, C. L.** (2014). Analysis of the Retromer complex-WASH complex interaction illuminates new avenues to explore in Parkinson disease. *Commun. Integr. Biol.*

**Shannon, B., Soto-Ortolaza, A., Rayaprolu, S., Cannon, H. D., Labbé, C., Benitez, B. A., Choi, J., Lynch, T., Boczarska-Jedynak, M., Opala, G., et al.** (2014). Genetic variation of the retromer subunits VPS26A/B-VPS29 in Parkinson's disease. *Neurobiol. Aging* **35**, 1958.e1-1958.e2.

**Small, S. A.** (2008). Retromer sorting: A pathogenic pathway in late-onset Alzheimer disease. *Arch. Neurol.* **65**, 323–328.

**Spinosa, M. R., Progida, C., De Luca, A., Colucci, A. M. R., Alifano, P. and Bucci, C.** (2008). Functional characterization of Rab7 mutant proteins associated with Charcot-Marie-Tooth type 2B disease. *J. Neurosci.* **28**, 1640–1648.

**Steinberg, F., Gallon, M., Winfield, M., Thomas, E. C., Bell, A. J., Heesom, K. J., Tavaré, J. M. and Cullen, P. J.** (2013). A global analysis of SNX27-retromer assembly and cargo specificity reveals a function in glucose and metal ion transport. *Nat. Cell Biol.* **15**, 461–471.

**Stewart, D. J., Short, K. K., Maniaci, B. N. and Burkhead, J. L.** (2019). COMMD1 and PtdIns(4,5)P2 interaction maintain ATP7B copper transporter trafficking fidelity in HepG2 cells. *J. Cell Sci.*

**Strochlic, T. I., Setty, T. G., Sitaram, A. and Burd, C. G.** (2007). Grd19/Snx3p functions as a cargo-specific adapter for retromer-dependent endocytic recycling. *J. Cell Biol.* **177**, 115–125.

**Suzuki, S. W. and Emr, S. D.** (2018a). Membrane protein recycling from the vacuole/lysosome membrane. *J. Cell Biol.* **217**, 1623–1632.

**Suzuki, S. W. and Emr, S. D.** (2018b). Retrograde trafficking from the vacuole/lysosome membrane. *Autophagy* **14**, 1654–1655.

**Suzuki, S. W., Chuang, Y. S., Li, M., Seaman, M. N. J. and Emr, S. D.** (2019). A bipartite sorting signal ensures specificity of retromer complex in membrane protein recycling. *J. Cell Biol.* **218**, 2876–2886.

**Tabuchi, M., Yanatori, I., Kawai, Y. and Kishi, F.** (2010). Retromer-mediated direct sorting is required for proper endosomal recycling of the mammalian iron transporter DMT1. *J. Cell Sci.* **123**, 756–766.

**Tammineni, P., Jeong, Y. Y., Feng, T., Aikal, D. and Cai, Q.** (2017). Impaired axonal retrograde trafficking of the retromer complex augments lysosomal deficits in Alzheimer's disease neurons. *Hum. Mol. Genet.* **26**, 4352–4366.

**Telianidis, J., Hung, Y. H., Materia, S. and Fontaine, S. La** (2013). Role of the P-Type ATPases, ATP7A and ATP7B in brain copper homeostasis. *Front. Aging Neurosci.* **5**,.

**Uauy, R., Olivares, M. and Gonzalez, M.** (1998). Essentiality of copper in humans. In *American Journal of Clinical Nutrition*, p. American Society for Nutrition.

**Vardarajan, B. N., Bruesegem, S. Y., Harbour, M. E., St. George-Hyslop, P., Seaman, M. N. J. and Farrer, L. A.** (2012). Identification of Alzheimer disease-associated variants in genes that regulate retromer function. *Neurobiol. Aging* **33**, 2231.e15-2231.e30.

**Wen, L., Tang, F. L., Hong, Y., Luo, S. W., Wang, C. L., He, W., Shen, C., Jung, J. U., Xiong, F., Lee, D. hoon, et al.** (2011). VPS35 haploinsufficiency increases Alzheimer's disease neuropathology. *J. Cell Biol.* **195**, 765–779.

**Zhang, J., Reiling, C., Reinecke, J. B., Prislan, I., Marky, L. A., Sorgen, P. L., Naslavsky, N. and Caplan, S.** (2012). Rabankyrin-5 Interacts with EHD1 and Vps26 to Regulate Endocytic Trafficking and Retromer Function. *Traffic* **13**, 745–757.

**Zhao, X., Nothwehr, S., Lara-Lemus, R., Zhang, B. Y., Peter, H. and Arvan, P.** (2007). Dominant-negative behavior of mammalian Vps35 in yeast requires a conserved PRLYL motif involved in retromer assembly. *Traffic* **8**, 1829–1840.

## Figures

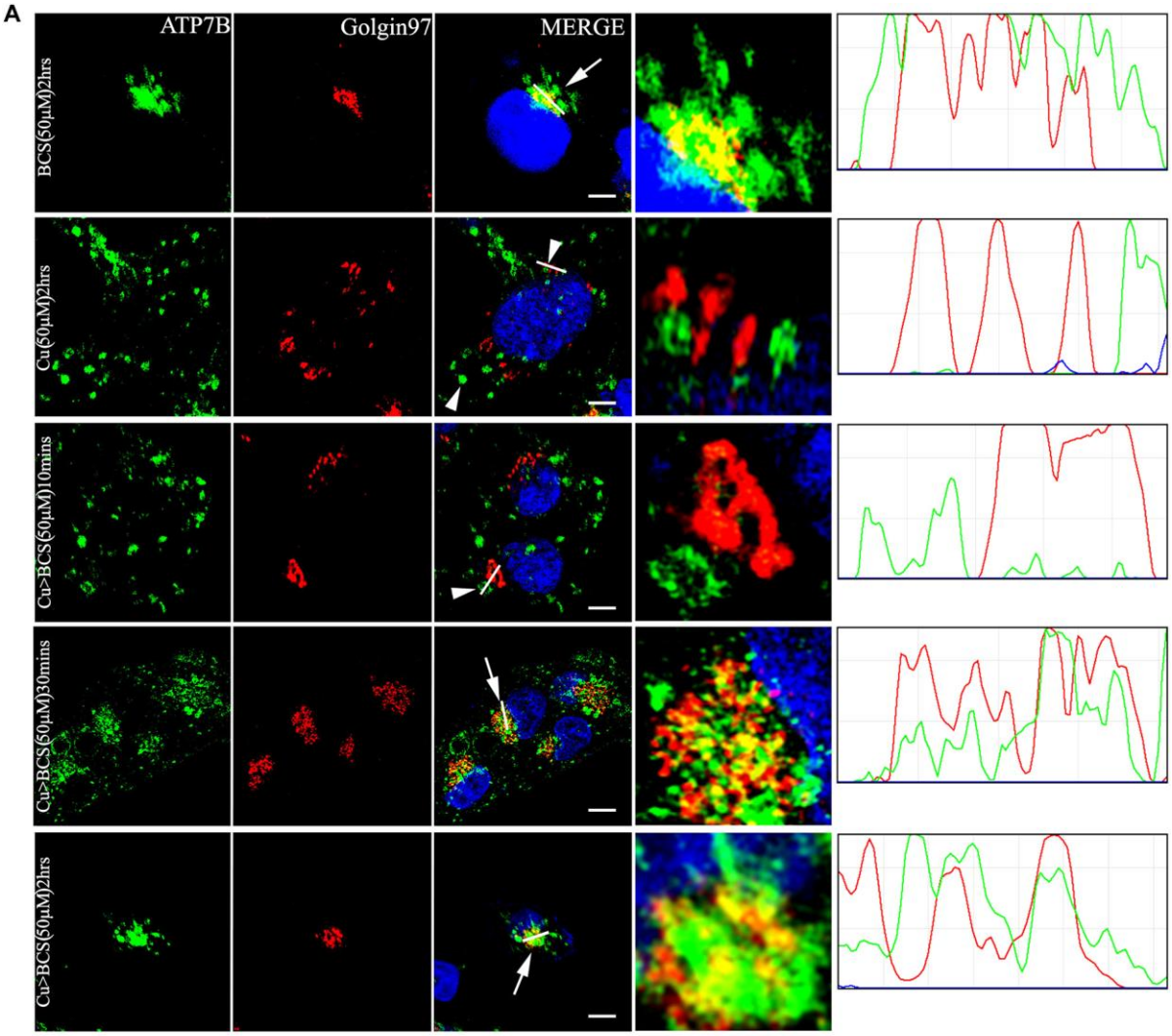


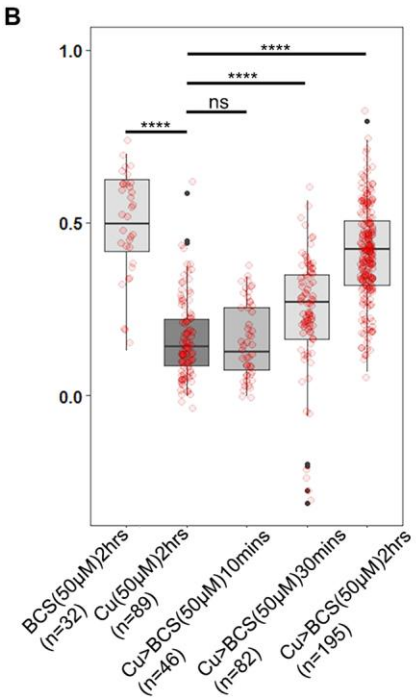

Fig.1: **ATP7B recycles between TGN and vesicles in a copper dependent manner:** (A) Colocalization of ATP7B (green) with TGN marker, Golgin97 (red) in copper limiting, BCS (top panel) and 50μM copper (panel 2). Panel 3-5 shows subsequent return of vesicularized ATP7B upon BCS treatment for varying time length (10, 30 and 120mins). The overlap plots (right boxes) show the extent of overlap of green and red at lines drawn through the signals located on TGN (marked by arrow or arrowhead). The line through the selected region of the image represents the overlap between green and red and has been magnified in the rightmost images. Arrow and Arrowhead represents TGN localized and vesicularized ATP7B respectively. Scale bars represents 5μM. Blue signal represents DAPI staining for nucleus. (B) Pearson's correlation coefficient of colocalization between ATP7B and Golgin97 at different copper conditions demonstrated by a box plot with jitter points. (**** $p<0.0001$). The number of cells counted to obtain the data for each condition is denoted by 'n'.

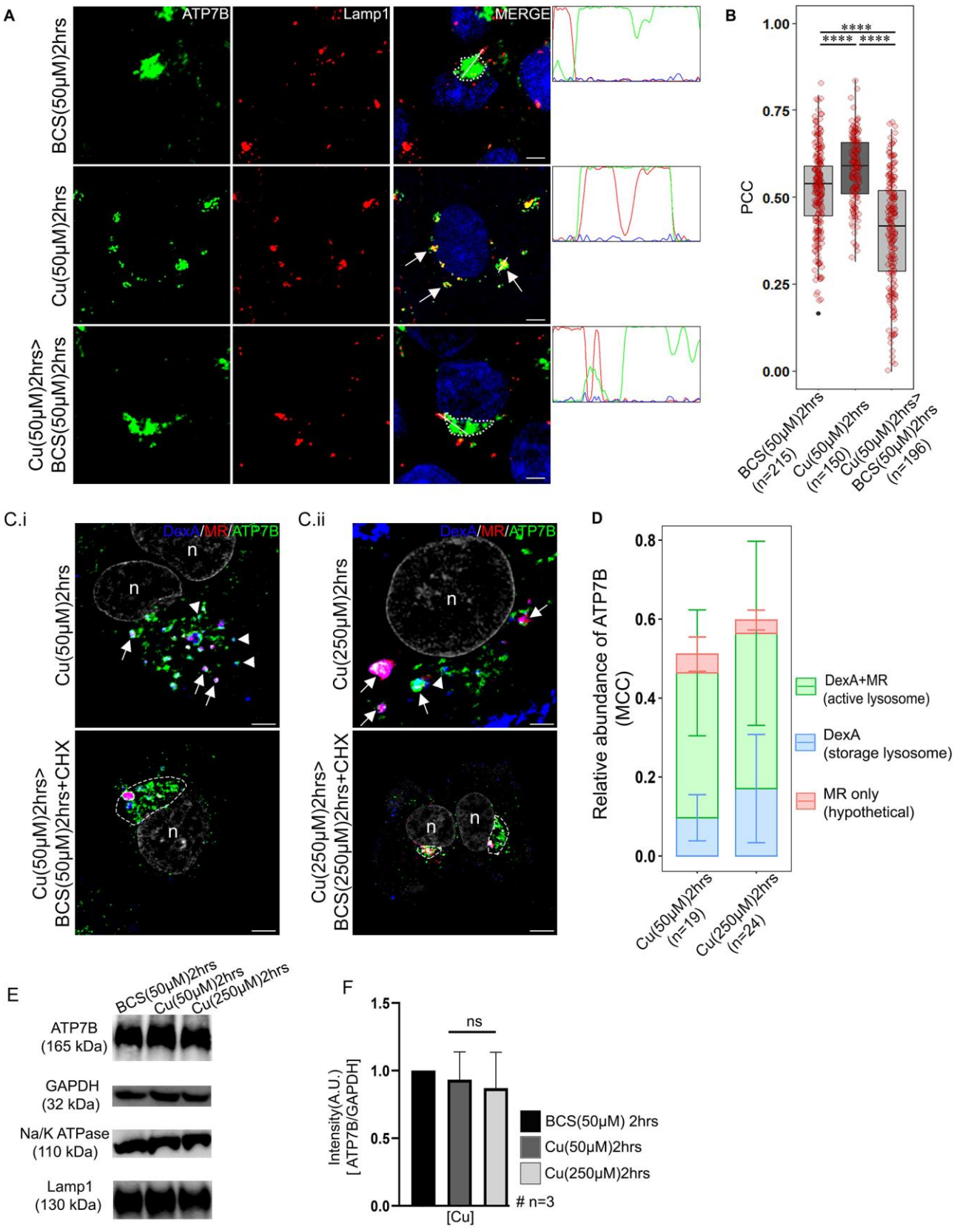


Fig.2: **ATP7B recycles from endolysosome upon copper depletion:** (A) Colocalization of ATP7B (green) with lysosomal marker, lamp1 (red) in copper limiting, BCS (top panel) and 50μM copper (panel 2) and copper depletion post copper treatment (bottom panel). The overlap plots (right boxes) show the extent of overlap of green and red at lines drawn through the signals (marked by arrow or arrowhead). Arrow represents vesicularized ATP7B and

dotted lines represents perinuclear positioned ATP7B. Scale bars represents 5µM. Blue signal represents DAPI staining for nucleus. (B) Pearson's correlation coefficient of colocalization between ATP7B and Lamp1 at different copper conditions demonstrated by a box plot with jitter points. (**** $p<0.0001$) (C) Colocalization of ATP7B (green), Alexa-647-Dextran (blue) and Magic Red, MR (red) in (C.i) 50µM copper (upper panel) and 50µM > 50µM BCS (lower panel) and (C.ii) 250µM copper (upper panel) and 250µM > 250uM BCS (lower panel) Arrow: ATP7B in active lysosomes; Arrowheads: ATP7B in storage lysosomes; Dashed line: Perinuclear concentration of ATP7B (D) Bar plot using Mander's colocalization coefficient (MCC) representing relative ATP7B localization in endolysosomes positive for both active acid-hydrolase and Dextran A (DexA+MR) and storage lysosomes exclusively positive for Dextran A (DexA). MR-only signal possibly represent background staining and falls within 5% range of error. 'n' denotes the nucleus (E) Immunoblot of ATP7B at different copper conditions (panel 1). GAPDH is used as a loading control (panel 2). Immunoblots of Lamp1 (panel 3) and Na,K-ATPase (panel 4) in different copper conditions. (F) Bar plot representing ATP7B abundance at different copper conditions as normalized against GAPDH abundance obtained from the respective immunoblots. The number of cells counted to obtain the data for each condition is denoted by 'n' (for B &D). Scale bars represents 5µM.

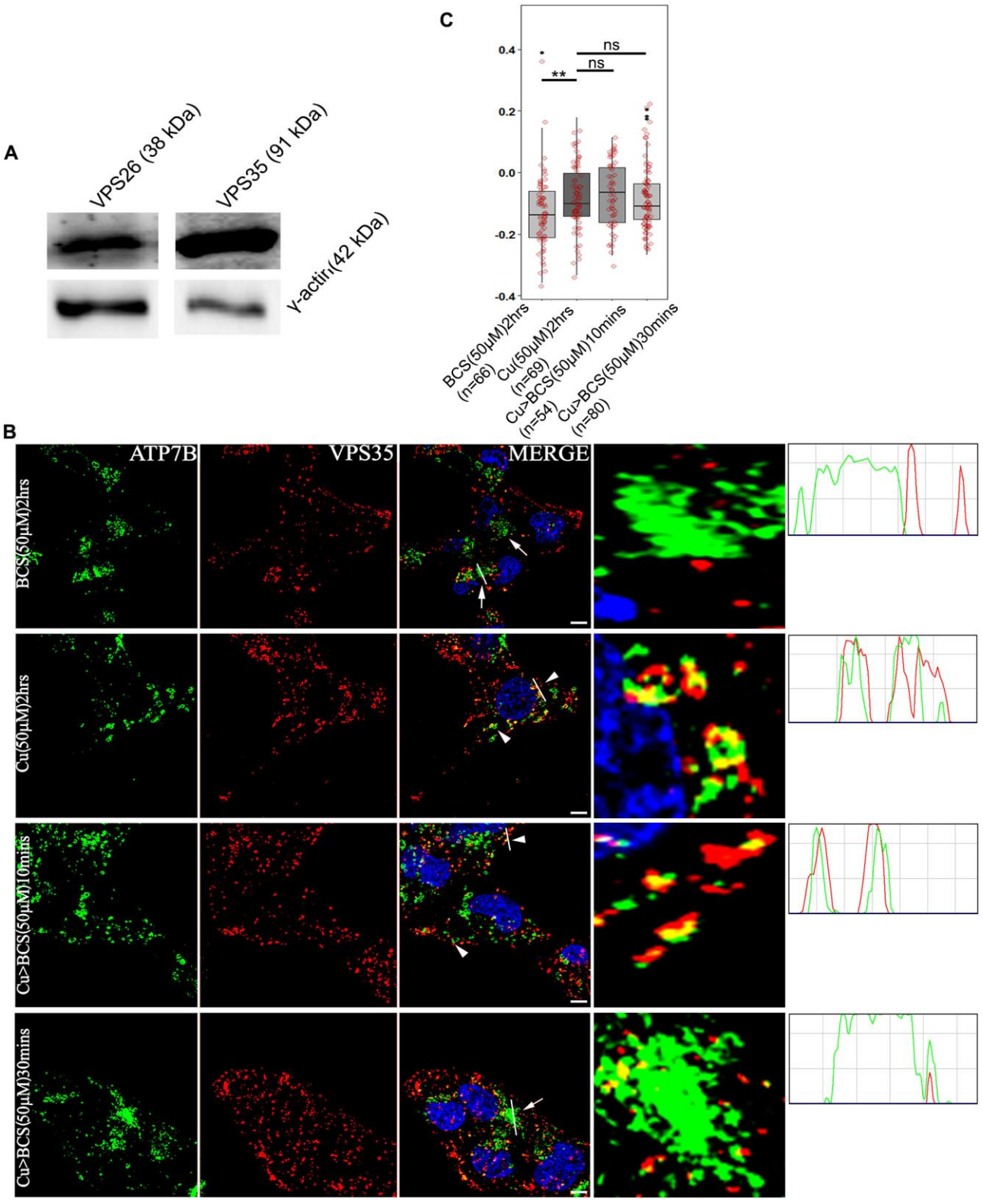


Fig.3: **ATP7B and VPS35 colocalizes at high copper:** (A) Immunoblot showing HepG2 expresses the retromer subunits VPS26 and VPS35 (top panel). ɣ-Tubulin is used as loading control (lower panel) (B) Colocalization of ATP7B (green) with retromer subunit, VPS35 (red) in copper limiting, BCS (top panel) and 50μM copper (panel 2) and copper depletion post copper treatment (panels 3-4). The overlap plots (right boxes) are from the region of the field has been magnified rightmost images) show the extent of overlap of green and red at lines drawn through the signals (marked by arrow or arrowhead). Arrowhead represents

vesicularized ATP7B and arrow represents perinuclear ATP7B. Line through the selected region of the image represents the overlap between green and red signals and has been magnified (rightmost image). Scale bars represent 5µM. Blue signal represents DAPI staining for nucleus. (C) Pearson's correlation coefficient of colocalization between ATP7B and VPS35 at different copper conditions demonstrated by box plot with jitter points (**$p<0.01$). The number of cells counted to obtain the data for each condition is denoted by 'n'.

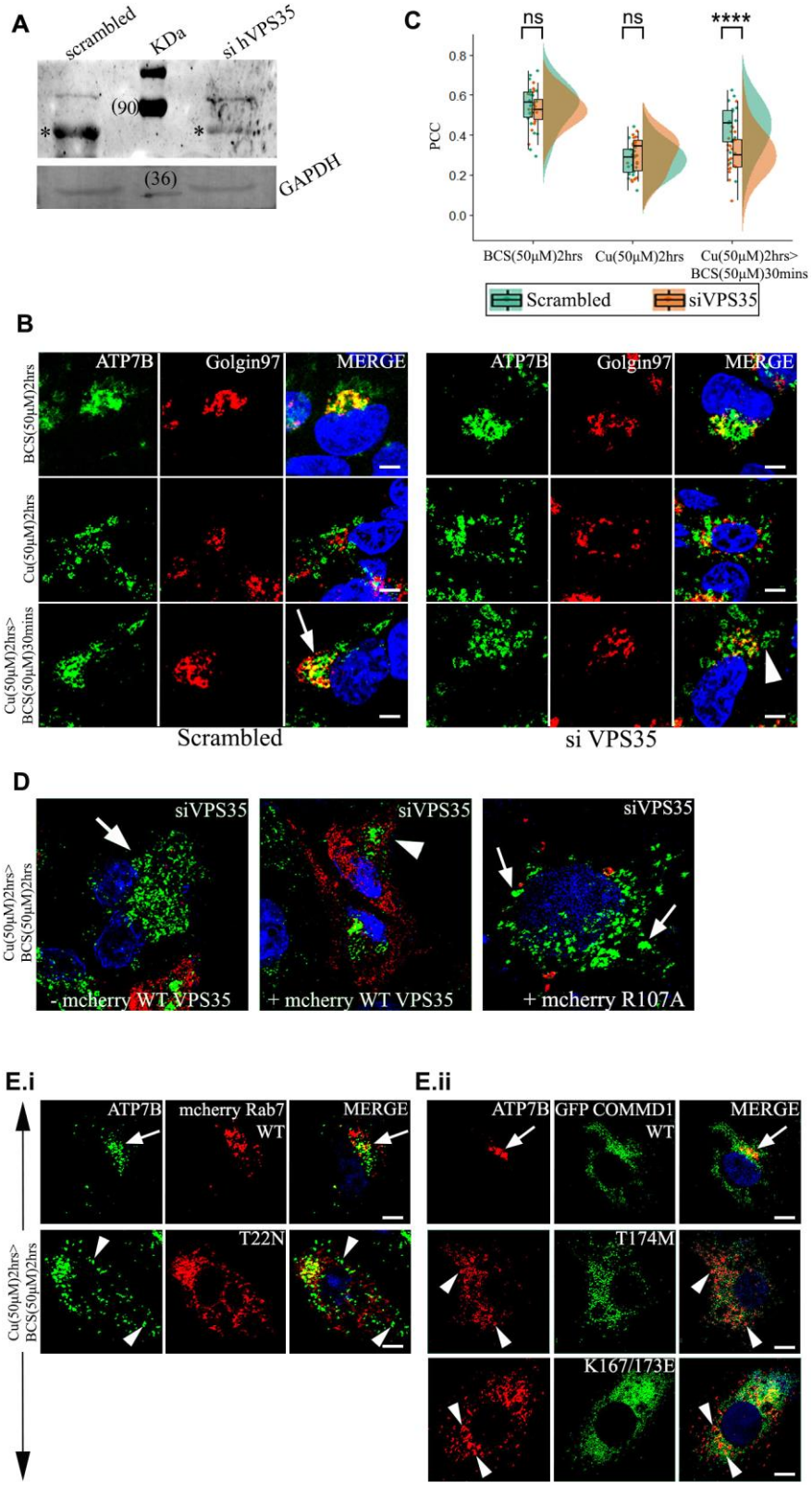


Fig.4: **VPS35 and its associated proteins regulates retrieval of ATP7B from lysosomes to TGN:** (A) siRNA mediated knockdown of Vps35 in HepG2 cells shows its downregulation. (*) denotes the VPS35 protein. GAPDH is used as a loading control. (B) Colocalization of ATP7B (green) with TGN marker, Golgin97 (red) in BCS (top panel) and 50μM copper (panel 2) and copper depletion post copper treatment (panels 3). Arrow denotes TGN colocalization of ATP7B, Arrowhead denotes vesicularized ATP7B. Scale bars represent 5μM. (C)

Pearson's correlation coefficient of colocalization between ATP7B and TGN at different copper conditions comparing VPS35 siRNA treated vs control demonstrated by a box plot. ($P<0.0001$) (D) Localization of ATP7B (green) in VPS35 siRNA treated cells and subsequently transfected with mCherry-wtVPS35 (red). The left image represents cells that is not expressing mCherry-wtVPS35 as compared to cells expressing mCherry-wt-VPS35 (center image) or the mutant, mCherry-R107A-VPS35 (right) (arrow: vesicularized ATP7B and arrowhead: tight perinuclear ATP7B). Cells belong to the same culture dish for both the left and center images. (E.i.) Localization of ATP7B (green) with cells overexpressing mCherry-wt-Rab7 (red) (top panel) or dominant negative mutant mCherry-T22N-Rab7 (bottom panel) in copper to BCS condition to triggers retrograde trafficking of ATP7B. (E.ii.) At the same copper condition as of E.i., localization of ATP7B (red) in cells overexpressing GFP-wt-COMMD1 (top panel) or the mutants GFP-T174M-COMMD1 (middle panel) and GFP-K167/173L-COMMD1 (bottom panel). Scale bars represents 5µM. Blue signal represents DAPI staining for nucleus.

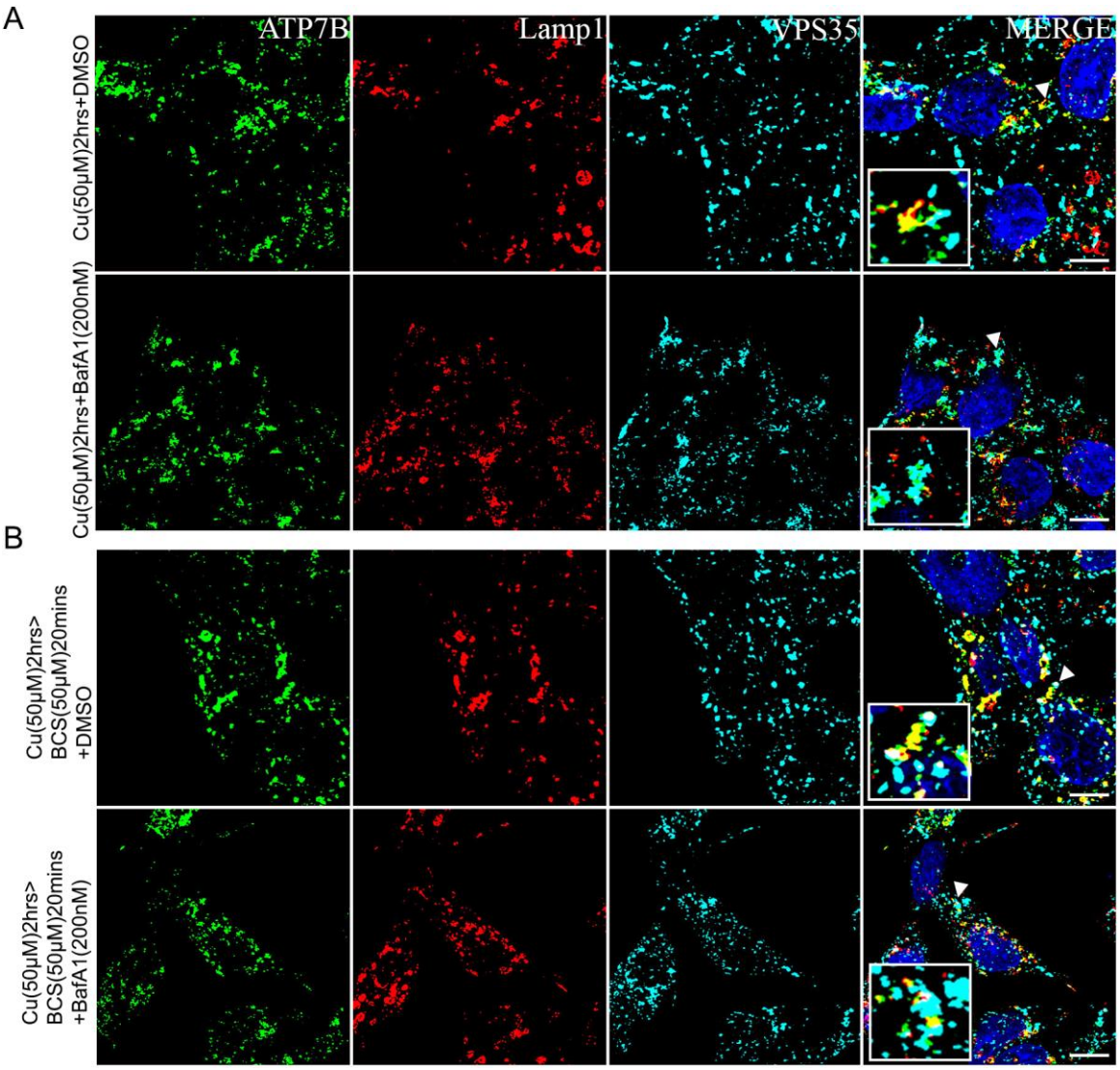


Fig.5: **Lysosomal luminal pH does not influence localization of ATP7B and recruitment of VPS35:** (A) Colocalization of ATP7B (green), Lamp1 (red) and VPS35 (cyan) in high copper for 2hrs in cells treated with Bafilomycin A1 (lower panel) or not (upper panel). (B) Colocalization of ATP7B (green), Lamp1 (red) and VPS35 (cyan) in cells treated with copper chelator for a brief period (20 mins) subsequent to high copper treatment to induce ATP7B vesicularization. Cells were treated with Bafilomycin A1 (lower panel) or not (upper panel). The magnified inset corresponds to the region of the main image marked by arrowheads. Scale bars represents 5μM.

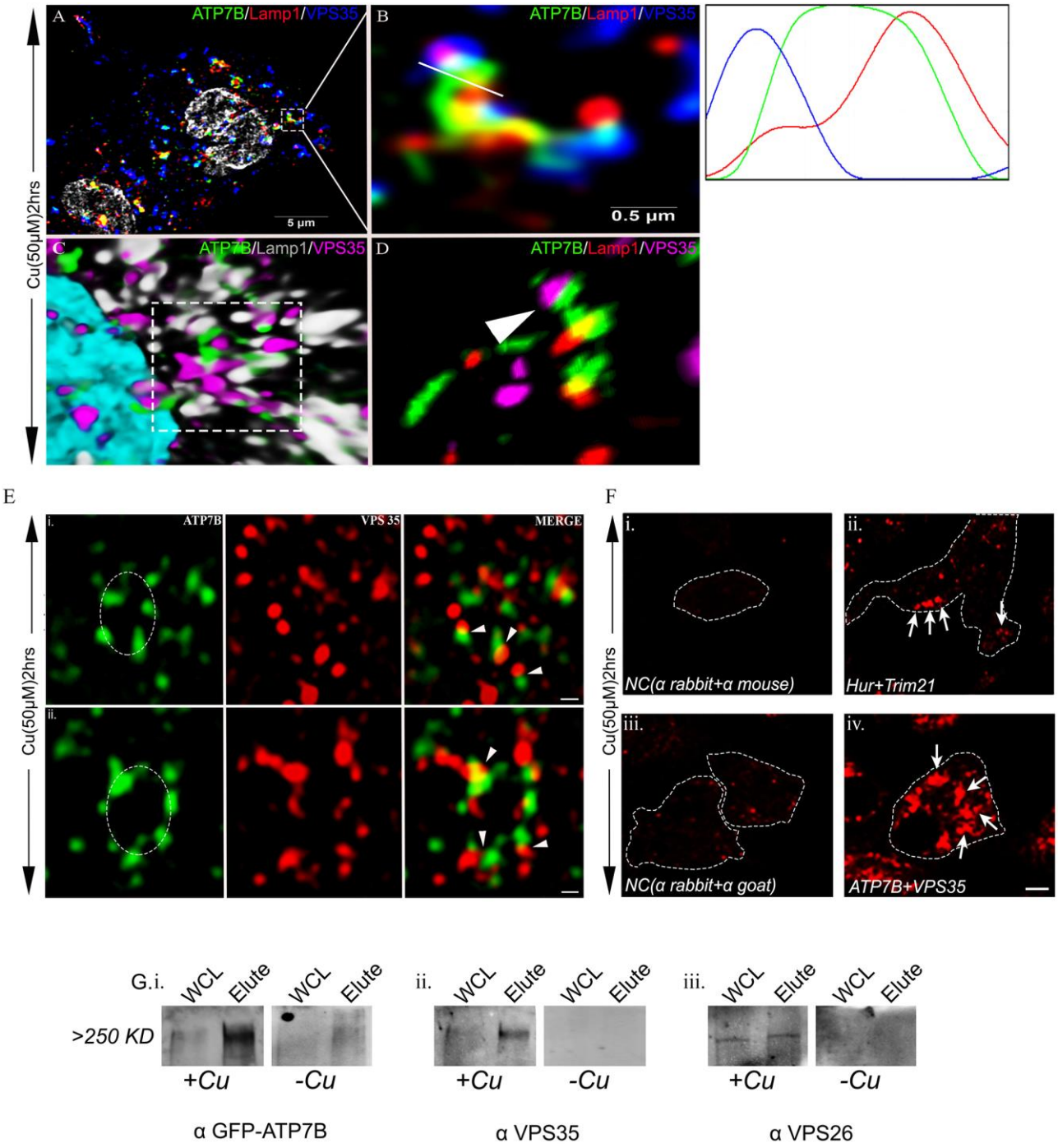


Fig.6: **VPS35 interacts with ATP7B on lysosome in a micro-distant manner:** (A) High resolution deconvoluted confocal microscopy merged image showing colocalization of ATP7B (green) with Lamp1 (red) and VPS35 (blue) at 50µM copper. Grey represents nucleus. (B) Zoomed image of inset in A. The overlap plots (right box) show the extent of overlap of green, red and blue at lines drawn through the signals (marked by white line). (C) 3D representation of zoomed image in B, marked by dashed line. ATP7B is marked in green, Lamp1 in grey, VPS35 in magenta. Cyan represents nucleus. (D) 3D representation of Structured Illumination Microscopy (SIM) image of same with 100nm resolution. ATP7B is marked in green, Lamp1 in red and VPS35 in magenta. Arrowhead represents co-distribution of ATP7B and VPS35 in lysosomal compartment (Lamp1). (E) Stimulated emission depletion (STED) microscopy image of ATP7B (green) and VPS35 (red). Both

panel represents colocalization of ATP7B and VPS35 in high copper. In both conditions ATP7B containing vesicles (marked by dotted circle) show juxta-positioning of VPS35 (red) and ATP7B (green). Arrowhead represents point of juxtaposition or merging. Scale bars represents 200nM. (F) Proximity Ligation Assay: *Upper panel* shows interaction of mouse Hur and rabbit Trim21 in HepG2 which serves as a positive control; **i.** Technical negative control (NC) without primary antibodies probed with only anti-rabbit(-) and anti-mouse(+) secondary PLA antibodies. **ii.** Hur and Trim21 interaction, marked by arrows. *Lower panel* shows interaction of rabbit ATP7B and goat VPS35 in HepG2; **iii.** Technical negative control (NC) without primary antibodies probed with only anti-rabbit(-) and anti-goat(+) secondary PLA antibodies. **iv.** ATP7B and VPS35 interaction, marked by arrows. (G) In- cell crosslinking A. Immunoblot showing presence of GFP both in WCL and elute in +Cu state at ~ >>250KDa (metabolically crosslinked with photo- amino acids) which was absent in –Cu state. B. and C. Similar pattern was observed for both co-eluted proteins VPS35 and VPS26 respectively; *WCL: Whole cell lysate*

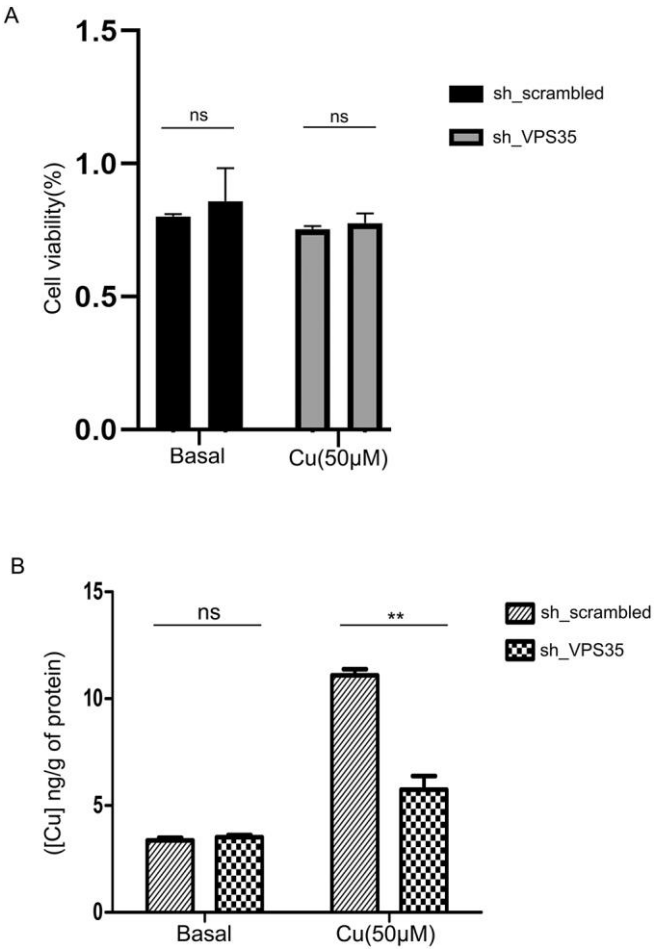


Fig.7: **Knocking down VPS35 does not affect cells viability but lowers intracellular copper content**. A. Graphical representation of cell viability where VPS35 expression was silenced by lentiviral mediated delivery of shRNA against VPS35 or not (non-targeting shRNA) as measured by neutral red (NR) assay. The assay was performed in two different copper conditions (basal and 50µM). Each conditions has 4 replicates ($p>0.1$) (B) Intarcellular copper content (ng/g) as measured by ICP-OES in cells subjected to identical knockdown or copper treatment conditions as of 7A. Each conditions has 5 replicates ($p<0.01$)

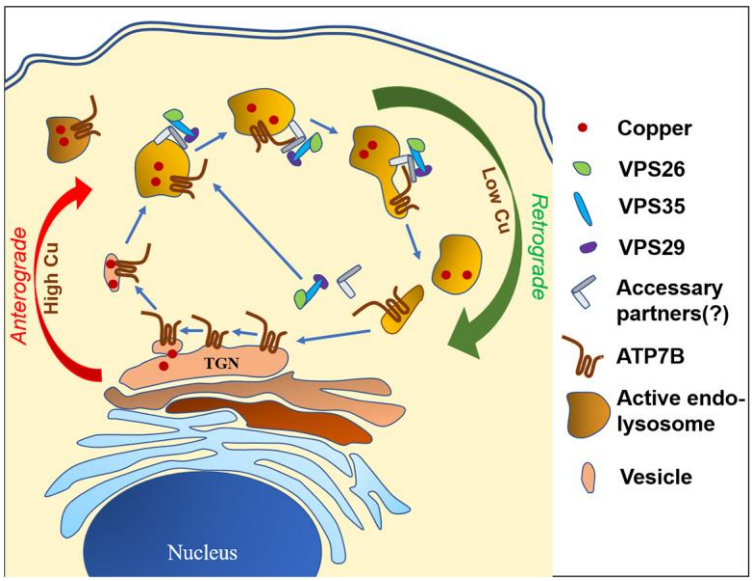


Fig.8: **Schematic representation of recycling of ATP7B between TGN and endolysosomes.** Retromers are recruited on the endolysosomal membrane that regulates retrograde transport of vesicularized ATP7B upon copper removal.

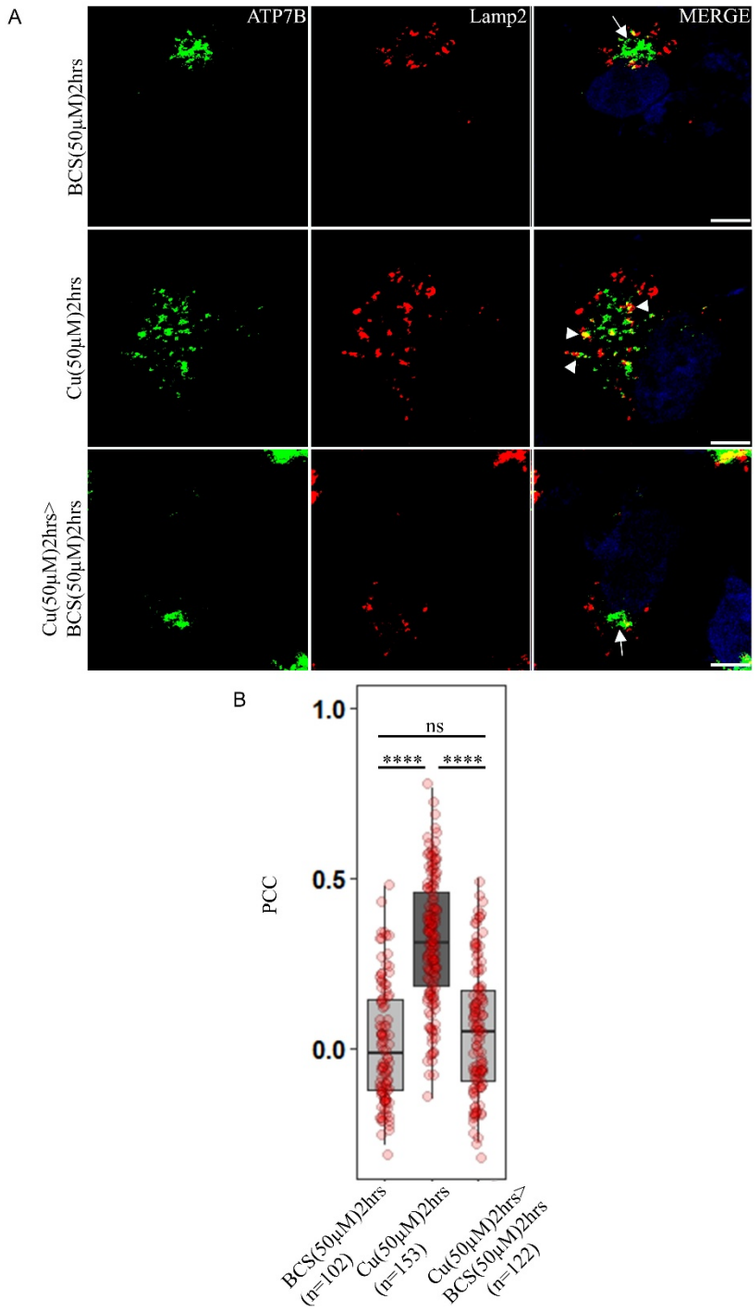


Fig. S1: Fig. S1: **ATP7B colocalizes with Lamp2 at high copper:** (A) Colocalization of ATP7B (green) with Lamp2 (red) in copper limiting, BCS (top panel) and 50µM copper (panel 2) and copper depletion post copper treatment (bottom panel). Arrowhead represents vesicularized ATP7B and arrows points at perinuclear positioned ATP7B. Scale bars represents 5µM. Blue signal represents DAPI staining for nucleus. (B) Pearson's correlation coefficient of colocalization between ATP7B and Lamp2 at different copper conditions demonstrated by a box plot with jitter points is illustrated at the bottom. ($p<0.0001$). The number of cells counted to obtain the data for each condition is denoted by 'n' (for B).

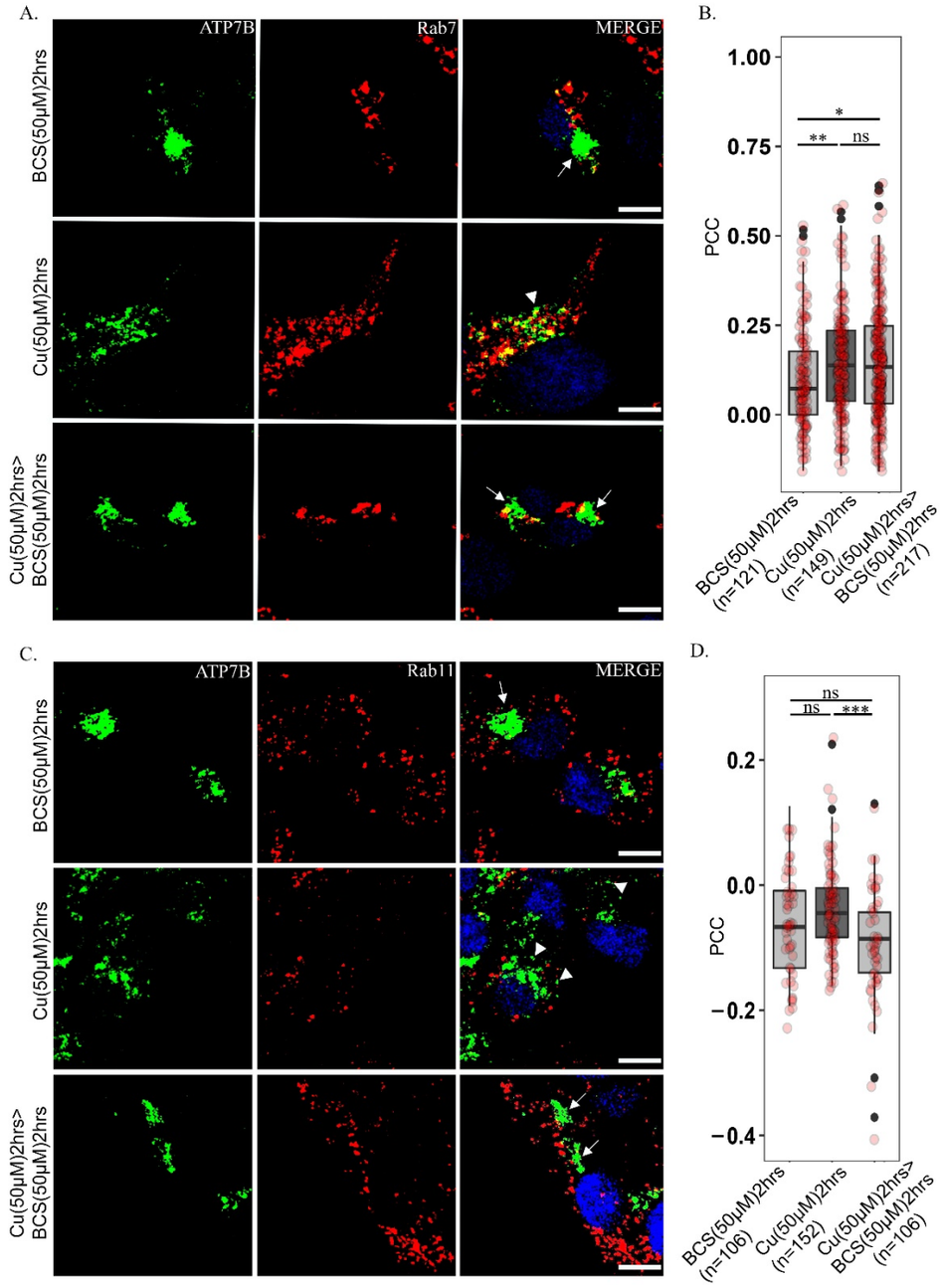


Fig. S2: **Colocalization of ATP7B with late (Rab7) and mid (Rab11) endosomal markers at different copper levels:** (A) Colocalization of ATP7B (green) with late endosome marker, Rab7 (red) in copper limiting, BCS (top panel) and 50uM copper (panel 2) and copper depletion post copper treatment (bottom panel). Scale bars represents 5μM. Blue signal represents DAPI staining for nucleus. (B) Pearson's correlation coefficient of colocalization between ATP7B and Rab7 at different copper conditions demonstrated by a box plot with jitter points. (C) Colocalization of ATP7B (green) with recycling endosomal marker, Rab11 (red) in different copper conditions (D) Pearson's correlation coefficient of colocalization between ATP7B and Rab11 at different copper conditions demonstrated by a box plot with jitter points. (*p<0.1, **p<0.01, ***p<0.001). The number of cells counted to obtain the data for each condition is denoted by 'n' (for B &D)

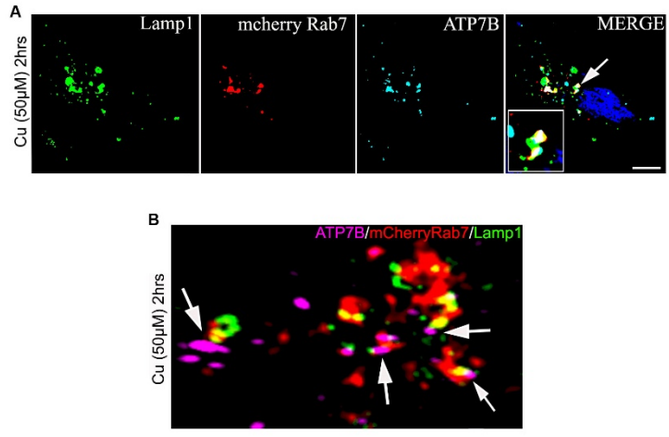


Fig. S3: **ATP7B is preferentially located in Rab7-Lamp1 positive endosomes in high copper**: (A) Colocalization of ATP7B (cyan) with lysosomal marker, lamp1 (green) and late endosome marker, mCherry Rab7 (red) at 50μM copper. The fig in the inset is representative of the region marked with an arrow. (B) 3D representation of Structured Illumination Microscopy (SIM) image of same with 100nm resolution. ATP7B is marked in magenta, Lamp1 in green and mCherry Rab7 in red. Arrow represents triple merging. Blue signal represents DAPI staining for nucleus. Scale bars represents 5μM

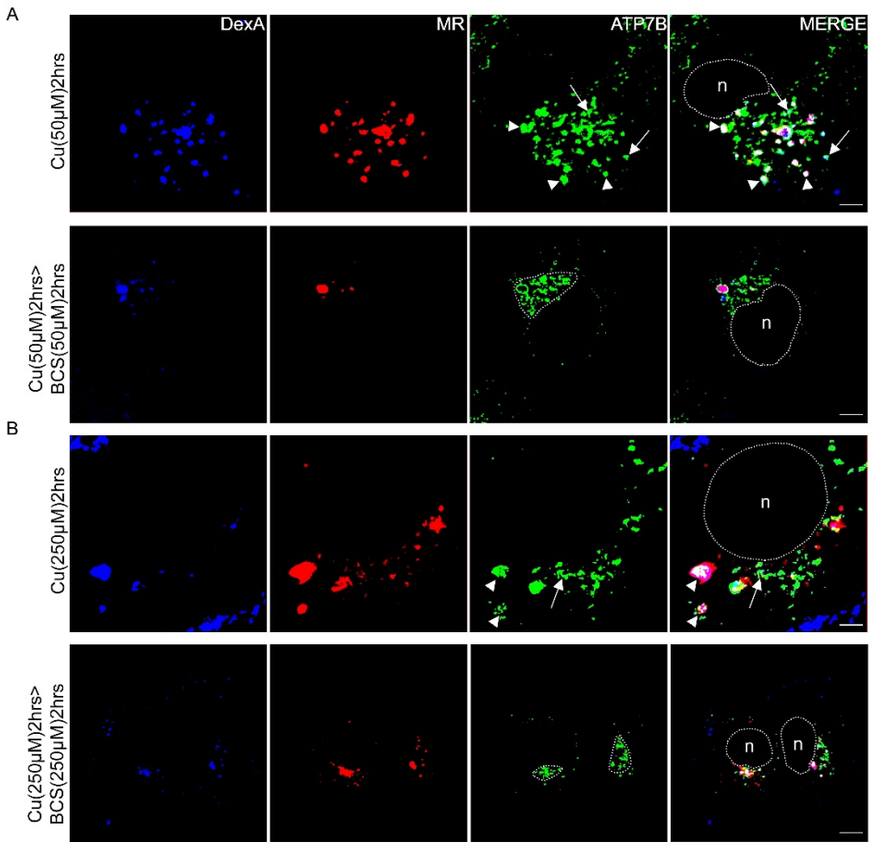


Fig. S4: **ATP7B shows preferential localization at acid-hydrolase positive endolysosomes at high copper:** Split channel illustration of Fig2 displaying colocalization of ATP7B (green), Alexa-647-Dextran (blue) and Magic Red, MR (red) in (A) 50μM copper (upper panel) and 50μM > 50μM BCS (lower panel) and (B) 250μM copper (upper panel) and 250μM > 250uM BCS (lower panel). Arrowhead: ATP7B in active endolysosomes and Arrow: ATP7B in storage lysosomes

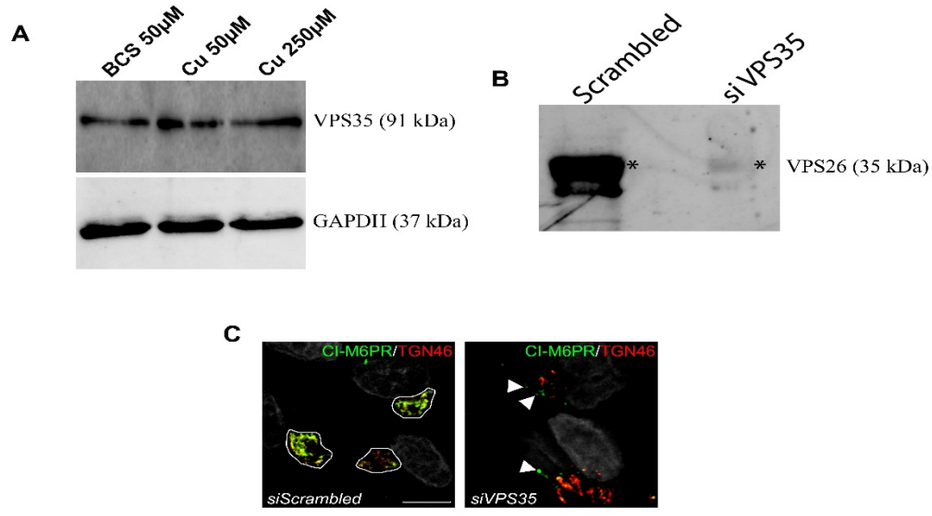


Fig. S5: (A) **Immunoblot of VPS35 in different Copper conditions:** Upper panel shows abundance of VPS35 remain unchanged in all copper conditions. Lower panel shows the same for GAPDH, as a control for cytosolic proteins. (B) **Immunoblot of VPS26 in siVPS35 HepG2:** siRNA mediated knockdown of Vps35 in HepG2 cells shows downregulation of its core partner VPS26 as compared to its control. (*) denotes the VPS26 protein. (C) **Knockdown of VPS35 abrogates recycling of CI-M6PR:** Colocalization of CI-M6PR (green) and TGN46 (red) in cells transfected with siRNA against VPS35 or scrambled siRNA (control). Vesicular puncta of CI-M6PR was noted in addition to its TGN localization in VPS35 KD cells, as against its complete localization in TGN in control cells

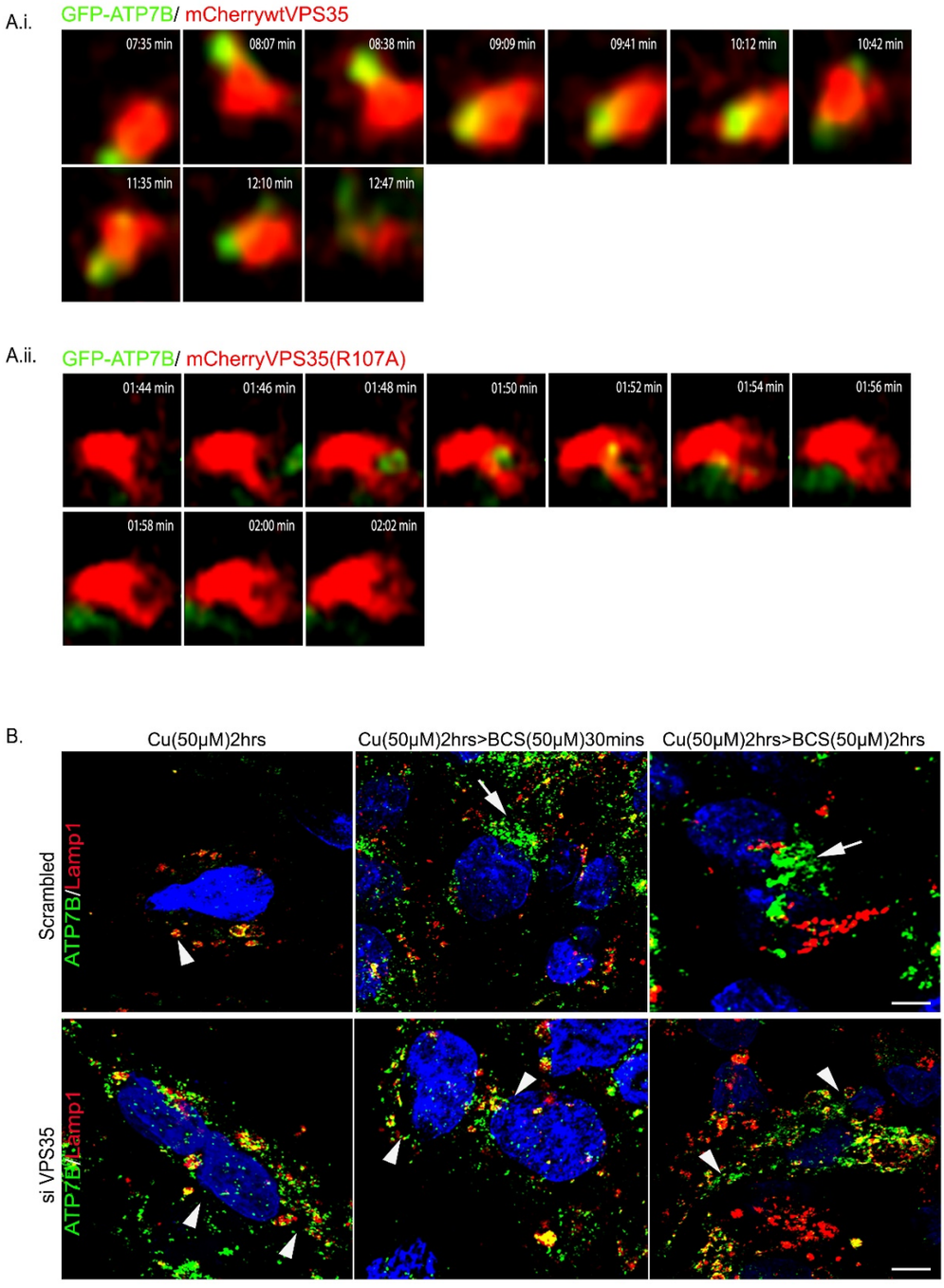


Fig. S6: **Comparative dwell time analysis of ATP7B and wtVPS35 vs its mutant, VPS35 R107A**: Live-cell time-lapse high resolution deconvolution confocal microscopy shows dwell time of GFP-ATP7B with mCherry VPS35-WT to be ≈ 4 mins (Ai) and for mutant ≈ 3 seconds (Aii) in 50uM copper. Images were taken at every 1.964 s interval. (B) **VPS35 regulates retrieval of ATP7B from endolysosome to TGN:** siVPS35 treated (bottom panel) and scrambled RNA treated (upper panel) HepG2 cell shows colocalization of ATP7B (green) with Lamp1 (red). Cells treated with copper for 2h (left image), subsequent copper depletion for 30 mins (center) and 2h (right image). Arrowhead shows ATP7B located in endolysosomal vesicles marked with Lamp1 and arrows shows perinuclear ATP7B indicative of its TGN localization. Scale bars represent 5μM. Blue signal represents DAPI staining for nucleus.

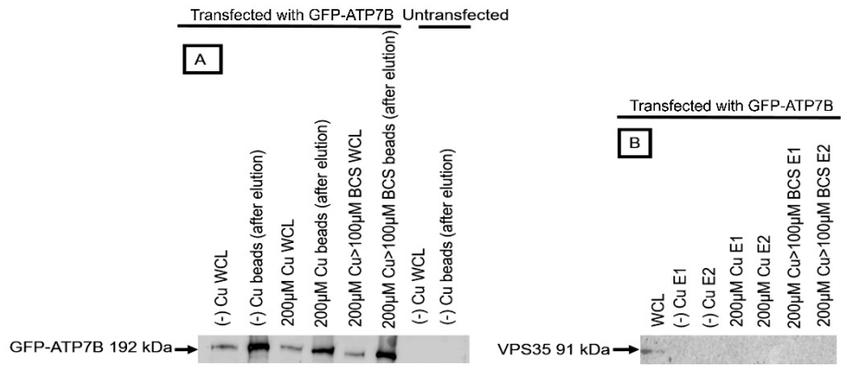


Fig. S7: **Co-immunoprecipitation assay to determine the interaction between full length ATP7B and VPS35:** Cell was transfected with GFP-ATP7B and treated with different copper conditions as mentioned. Lysates were incubated with GFP-trap beads. Untransfected cells were used as negative control. (A) Immunoblot showing the presence of GFP-ATP7B in whole cell lysates and GFP-trap beads after elution. (B) GFP-trap immune-co-precipitated products were subjected to immunoblot as indicated. Abbreviations: *FT: Flow through; WCL: Whole cell lysate, E: Eluate.*

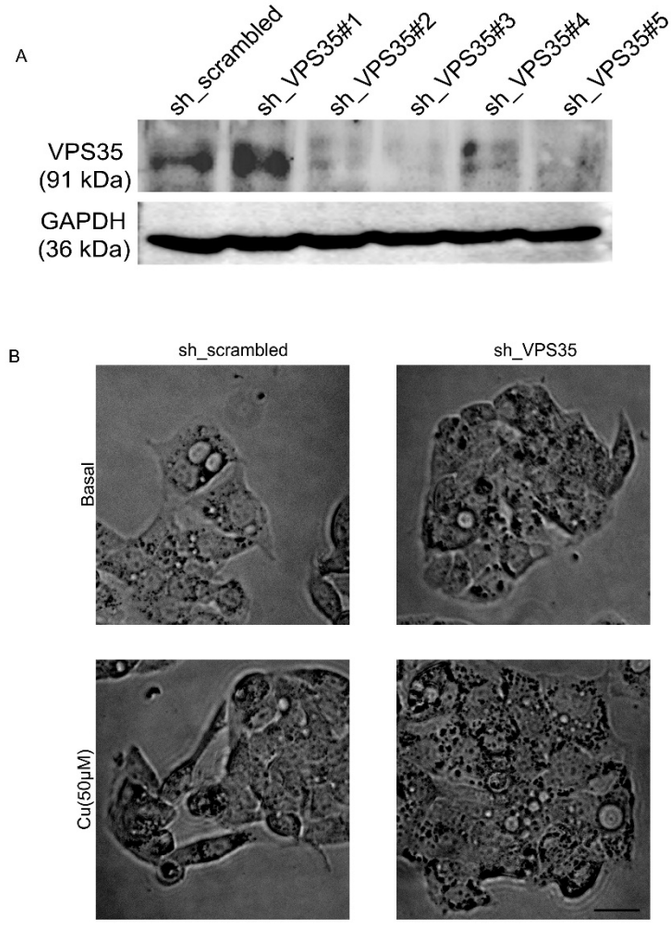


Fig. S8: (A) **shRNA mediated VPS35 knockdown:** VPS35 knockdown in HepG2 cells using lentivirus mediated delivery of 5 different shRNA targeted against 5 unique regions of the gene. shRNA #2,3 and 5 shows robust knockdowns. GAPDH is used as a control. These were subsequently used in experiments. (B) **Cell morphology using bright field images** of HepG2 cells: no apparent change in the cell morphology was noticed in cells with VPS35 expression silenced by lentiviral mediated delivery of shRNA (right images, top and bottom) or not (non-targeting shRNA) (left, top and bottom) in two different copper conditions. Scale bar represents 100 μM.

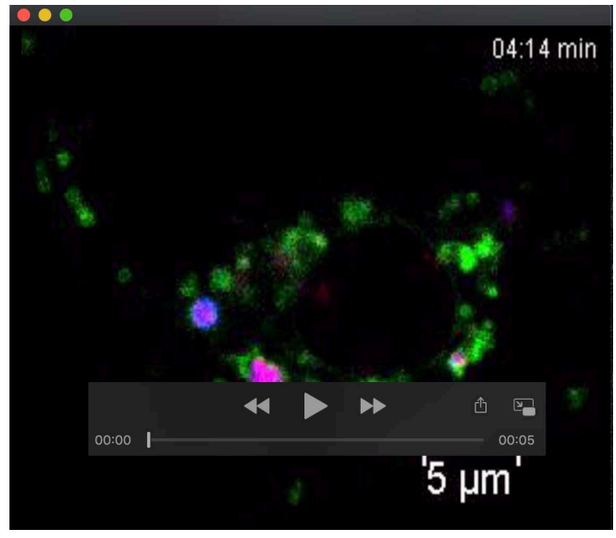


Movie 1: Time lapse imaging to record colocalization of ATP7B (green), Magic red (red) and DexA (blue) in high copper.

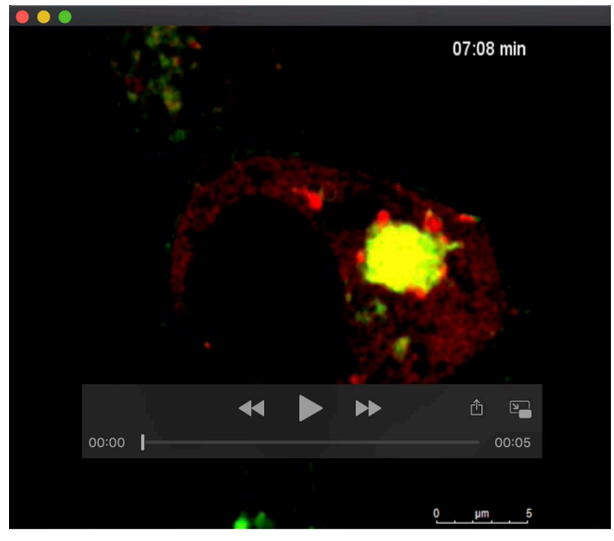


Movie 2A: Time lapse imaging to record colocalization of GFP-ATP7B (green) and mCherry-wt-VPS35 (red) in high copper.

Journal of Cell Science • Supplementary information

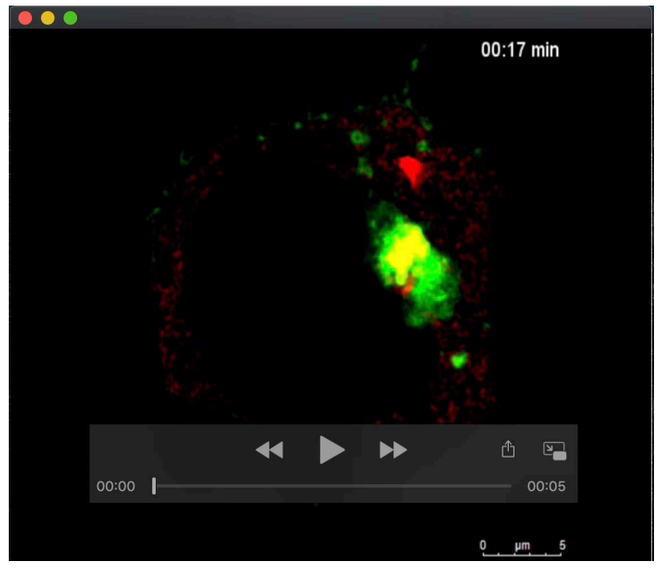


Movie 2B: Time lapse imaging to record colocalization of GFP-ATP7B (green) and mCherry-R107A-VPS35 (red) in high copper.